ANTIOXIDANTS & REDOX SIGNALING
Volume 13, Number 5, 2010

DOI: 10.1089/ars.2009.2948

COMPREHENSIVE INVITED REVIEW

Fluorescent Protein-Based Redox Probes

Andreas J. Meyer[1] and Tobias P. Dick[2]

Abstract

Redox biochemistry is increasingly recognized as an integral component of cellular signal processing and cell fate decision making. Unfortunately, our capabilities to observe and measure clearly defined redox processes in the natural context of living cells, tissues, or organisms are woefully limited. The most advanced and promising tools for specific, quantitative, dynamic and compartment-specific observations are genetically encoded redox probes derived from green fluorescent protein (GFP). Within only few years from their initial introduction, redox-sensitive yellow FP (rxYFP), redox-sensitive GFPs (roGFPs), and HyPer have generated enormous interest in applying these novel tools to monitor dynamic redox changes *in vivo*. As genetically encoded probes, these biosensors can be specifically targeted to different subcellular locations. A critical advantage of roGFPs and HyPer is their ratiometric fluorogenic behavior. Moreover, the probe scaffold of redox-sensitive fluorescent proteins (rxYFP and roGFPs) is amenable to molecular engineering, offering fascinating prospects for further developments. In particular, the engineering of redox relays between roGFPs and redox enzymes allows control of probe specificity and enhancement of sensitivity. Genetically encoded redox probes enable the functional analysis of individual proteins in cellular redox homeostasis. In addition, redox biosensor transgenic model organisms offer extended opportunities for dynamic *in vivo* imaging of redox processes. *Antioxid. Redox Signal.* 13, 621–650.

Reviewing Editors: *Shawn C. Burdette, Salvatore Cannistraro, Pier G. Mastroberardino, and S. James Remington*

[1]Heidelberg Institute for Plant Science, Heidelberg University, Heidelberg, Germany.
[2]German Cancer Research Center, DKFZ-ZMBH Alliance, Heidelberg, Germany.

I. Introduction: Redox Biosensing Between Aspiration and Reality

The last few years have seen quite a change in the perception of the role of reactive oxygen species (ROS) in biological systems. It has become clear that ROS are produced in many physiological situations, and that they can act as messengers in signal transduction (22). In particular, hydrogen peroxide (H_2O_2) has emerged as a widespread, physiologically relevant and selective signaling molecule (119). H_2O_2 takes part in signaling by reversibly modifying critical thiol groups in a range of signaling proteins. Endogenous changes of oxidant levels are now recognized to fulfill positive functions in that they contribute to cell fate decisions, such as proliferation, differentiation, and apoptosis. The duality of oxidant action (adaptive vs. damaging) likely represents a challenge for biological systems, namely to allow for oxidative sensing and signaling on the one hand but to restrict uncontrolled oxidation on the other (130). Not surprisingly, oxidative processes are frequently found at the boundary between physiological and pathophysiological processes. Despite considerable interest and effort, the causal relationships between oxidants, redox homeostasis and disease have remained largely elusive. It appears likely that fundamental progress will depend on the development of high-precision tools for the quantitation and experimental manipulation of defined redox processes *in vivo*.

A. The need for novel redox probes

The study of redox processes in biological systems is a very broad and diverse field. It is always complex, frequently unclear, and sometimes downright confusing. One factor contributing to widespread confusion is the conceptual lumping together of diverse redox processes, as if they could be treated as one entity. Terms such as "cellular redox state" or "redox environment" are frequently used without further definition. Such terms seem to imply that a redox state is something like a global characteristic that does not require reference to any specific redox pair, or that the different redox pairs of the cell are in thermodynamic equilibrium, so that one redox pair can be used as a proxy for all the others. Such implicit assumptions are highly unrealistic. Cells harbor a multitude of redox pairs which are kinetically controlled and far from equilibrium with each other. Many kinds of redox reactions are thermodynamically favored, yet kinetically, sterically, or compartmentally separated. The enzymatic by-passing of kinetic inhibition is a powerful and fast-acting control principle in biology. The function of redox catalysts is to allow thermodynamic equilibration between two redox pairs in the right place and at the right time. For example, NADPH oxidase enzymes act as a highly regulated kinetic passageway for electron transfer between $NADPH/NADP^+$ and $O_2/O_2^{\bullet-}$ (63). Because of barriers and their selective suspension by catalysts, the spatio-temporal pattern of intracellular redox changes

is highly nonuniform between and within cellular compartments. Likewise, it is increasingly recognized that individual redox systems have distinct functions and are subject to independent regulation. Thus, a key task is to define the functional role of individual redox systems by looking at them specifically.

We are now at a stage where long-cherished views about "oxidants," "oxidative stress," and "antioxidants," and their relationship with organismal health, are increasingly being questioned. Beneficial roles of oxidants (90, 94), and potentially harmful effects of antioxidants (99, 104) continue to be recognized. Obviously, broad concepts and umbrella terms (like "oxidative stress," "ROS," and "antioxidants") lack the conceptual acuity that is needed for the understanding of the underlying causal relationships. After all, most cellular redox couples entertain electron transfer relationships in a dynamic and context-dependent manner. Obviously, a fine-grained view is needed, namely the quantitative measurement of clearly defined individual redox relationships in their specific cellular context, with high spatio-temporal resolution. Unfortunately, our ability to do this is very much limited.

Consequently, the redox probes we seek for the future must be highly specific for defined individual redox-active species or redox pairs. By responding sensitively, instantaneously, and reversibly, these probes have to allow compartment-specific real-time measurements in living cells, tissues, and whole organisms. They should not perturb cellular behavior and be easy to use. As if that were not demanding enough for a single probe, a whole collection of such redox probes will be needed, covering the spectrum of biologically relevant redox active molecules and redox pairs. High on the wish-list are probes for superoxide ($O_2^{\bullet-}$), H_2O_2, nitric oxide ($NO^{\bullet}$), glutathione (reduced form: GSH; oxidized form: GSSG), and ascorbate (reduced form: AA; oxidized form: dehydroascorbate, DHA). Not least, the redox status of proteins involved in the transmission of redox signals such as oxidoreductases (*e.g.*, thioredoxin) and peroxidases (*e.g.*, peroxiredoxins) is of fundamental interest as well.

B. The limits of conventional redox measurements

This review is about genetically encoded redox probes, because they promise to overcome many of the problems associated with conventional redox measurements. Briefly, these problems fall into two broad categories. The first major problem relates to the disruption of cells. Examples are measurements of glutathione, ascorbate, NADPH, and thioredoxin (Trx), by use of enzymatic assays, HPLC, or gel mobility. The major advantage is high specificity for the redox couple in question. Typically, both the oxidized and reduced form can be quantified and redox potentials estimated. The major disadvantage though is cell disruption, which creates oxidation artifacts, precludes dynamic measurements, and implies that calculated redox potentials are at best apparent redox potentials lacking resolution for specific subcellular compartments. For example, while several glutathione assays are reproducible and statistically robust, they all suffer from the inherent problem that tissue extraction and cellular disruption unavoidably destroys information about compartment-specific glutathione redox states.

The second major problem relates to the limitations of redox-active fluorogenic dyes when they are applied to living cells. Thiol-reactive dyes allow estimation of cellular glutathione content but cannot deliver information about the redox state of the glutathione couple (4, 81, 114, 134). Most oxidant-sensitive fluorescent dyes are characterized by at least partial nonspecific behavior, irreversibility, and lack of compartment specificity. The most widespread method to detect H_2O_2 in intact cells is the oxidation of 2′,7′-dihydrodichlorofluorescein (H_2DCF) to the fluorescent compound 2′,7′-dichlorofluorescein (DCF). However, oxidation of H_2DCF can occur in the absence of H_2O_2 and is stimulated by metals, peroxidases, and cytochrome c (102, 115). Like many other oxidant-sensitive dyes, H_2DCF can only be considered a qualitative marker of undefined pro-oxidative processes. However, it should be noted that improved chemical probes are now being developed. For example, Christopher Chang and colleagues synthesized probes that are specifically triggered by H_2O_2 (16, 83, 85) and reversibly reacting probes that enable dynamic measurements (84, 86). Advanced chemical probes are thus prone to play important roles in the future and should be considered complementary to the fluorescent protein-based redox probes which are the subject of this review.

II. Redox-Sensitive Fluorescent Proteins

Although considerable progress is being made in the development of chemical probes (86), there are still major limitations regarding reversibility, quantitation, and subcellular targeting. Many of these limitations were overcome by the development of the first genetically encoded redox probes that allowed the quantitation of a dithiol–disulfide equilibrium within live cells. Green fluorescent protein (GFP) and its variants are resistant to common proteases and stable under physiological pH conditions, thus providing an excellent scaffold for the development of biosensors for physiologically important parameters. Therefore, it is not surprising that GFP attracted major interest for the development of redox-sensitive probes, which are now about to transform redox research towards more quantitative and dynamic approaches. The groups of Jakob Winther and James Remington independently developed GFP-based redox-sensitive probes by placing artificial disulfides onto fluorescent protein (FP) scaffolds. Redox-sensitive yellow fluorescent protein (rxYFP) and redox-sensitive GFP (roGFP) both allow noninvasive quantitative imaging of the associated dithiol–disulfide equilibrium (27, 92, 93). The set of redox-sensitive FPs was recently supplemented with a circularly-permuted YFP variant (cpYFP), which appears to be responsive to $O_2^{\bullet-}$ (126). Here, we will discuss the properties and some applications for these probes.

A. Common properties of FPs

Wild-type GFP (wtGFP), originally isolated from the jellyfish *Aequorea victoria* by Osamu Shimomura (111), is a soluble protein of 27 kDa. The 238 amino acid long polypeptide forms an 11-stranded β-barrel shielding an internal α-helix, which runs up the axis of the β-barrel, against the surrounding medium (91, 133). The wild-type chromophore of GFP is formed through intramolecular cyclization of the three amino acids S65/Y66/G67 (Fig. 1A). Subsequent oxidation leads to formation of a conjugated system of π-electrons capable of absorbing and emitting visible light. Wild-type GFP has two excitation peaks which reflect different protonation states of the phenol group of Y66 within the chromophore (Fig. 1B), but

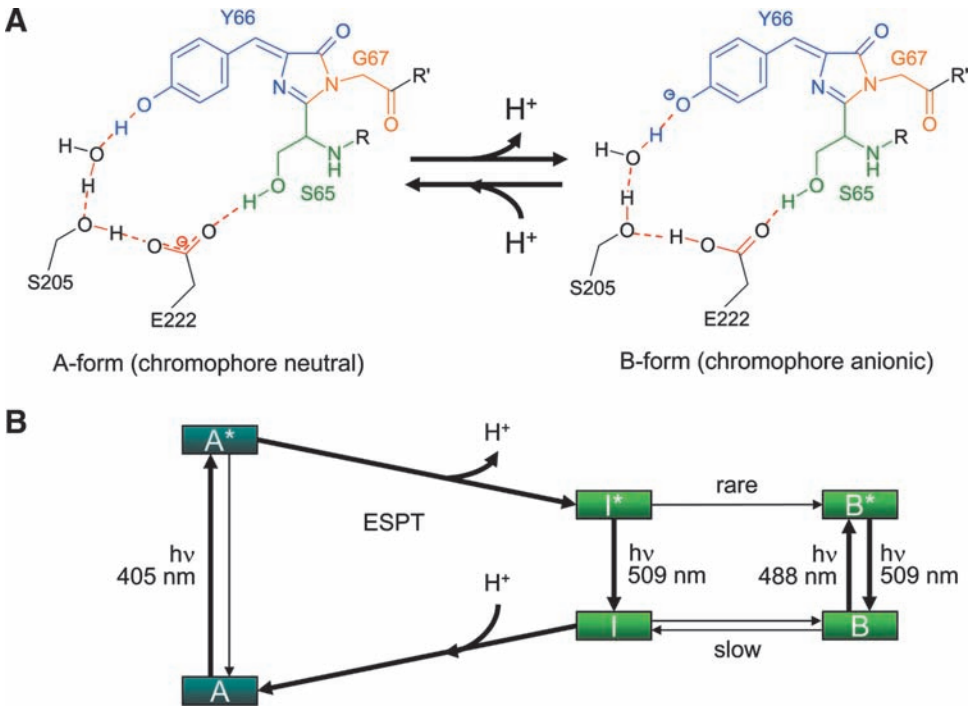

FIG. 1. Reversible deprotonation of the GFP chromophore gives rise to two distinct excitation maxima. (**A**) Interconversion of the chromophore between the neutral A-Form and the anionic B-form. The chromophore is formed from S65 (*green*), Y66 (*blue*), and G67 (*red*). Deprotonation of the phenolic hydroxyl group is coupled to protonation of E222 through an H-bonding network that involves S65, S205, and a structural water molecule. (**B**) Excited state proton transfer (ESPT) converts the neutral A-form of GFP to the anionic I-form. Excitation wavelengths 405 and 488 nm, respectively, refer to the main laser lines used for confocal ratio imaging. Modified from (78). (For interpretation of the references to color in this figure legend, the reader is referred to the web version of this article at www.liebertonline.com/ars).

only a single emission peak with a maximum at 509 nm. The first excitation peak with a maximum at 395 nm corresponds to the protonated neutral form of the chromophore (A-band) and the second peak with a maximum at 475 nm corresponds to the de-protonated, anionic form (B-band) (9, 30). Following excitation at the A-band (*e.g.*, with the laser wavelength 405 nm) the excited neutral chromophore (A*) converts to the unrelaxed anionic form (I*) by transferring the phenolic proton from Y66 to the carboxylate of E222. This process is called excited state proton transfer (ESPT) (17) and involves a hydrogen bonding network surrounding the chromophore. The proton transfer between Y66 and E222 is mediated by a structural water molecule and the hydroxyl group of S205 (Fig. 1A). ESPT is the reason why excitation at both bands leads to emission of green light of similar wavelength (Fig. 1B) (78). Importantly, the dual excitation-single emission behavior of GFP can be exploited for ratiometric measurements.

In general, the degree of chromophore protonation is determined through interactions with the surrounding residues and thus can be affected by changes in protein composition and structure. The most relevant amino acids are those involved in the ESPT hydrogen bonding network (*i.e.*, S205, E222, S65) and those in close proximity of Y66 (*i.e.*, N146, H148, T203). For instance, chromophore deprotonation is significantly favored when S65 is replaced by threonine. The S65T mutation, leading to enhanced GFP (EGFP), thus shifts the major excitation peak to 488 nm (53). On the other hand, a way to manipulate FP emission is to alter chromophore stacking interactions. In YFP, the additional T203Y mutation leads to π-electron stacking between the chromophore and the aromatic side chain of Y203 (117, 124). Although generally considered to be a very rigid structure, the β-barrel has some flexibility and minor conformational changes can lead to alterations in chromophore protonation or π-electron stacking. Such changes have been exploited in roGFP and rxYFP.

B. Probes with disulfide bonds engineered into the GFP β-barrel

1. rxYFP. The introduction of the T203Y mutation converted EGFP to YFP, a red-shifted GFP variant with an excitation maximum at 513 nm and emission at 527 nm (124). Based on the assumption that dislocation of Y203 and accompanying changes in π-electron stacking would affect fluorescence significantly, Ostergaard and colleagues used YFP as a template for redox-sensitive variants (rxYFP) (92). Dislocation of Y203 was expected to occur when the β-strand 10 (aa 199–208) of the β-barrel of the YFP protein was forced into a slightly different position. To achieve such conformational change, pairs of cysteines were introduced in different positions on β-strands 7 and 10 such that the two residues are capable of forming an intramolecular disulfide bridge. Of four different combinations of cysteine pairs only the variant N149C/S202C gave a strong redox-dependent change in fluorescence (92). Formation of the disulfide bond between these two cysteines resulted in a 2.2-fold reduction of the emission peak without a significant shift in the excitation wavelength. YFP exhibits two absorption peaks for the neutral A-band ($\lambda_{max} = 392$ nm) and the anionic B-band ($\lambda_{max} = 514$ nm), with a clean isosbestic point at 432 nm (125). However, due to fluorescence quenching, the neutral form of YFP is nonfluorescent and thus recombinant rxYFP exhibits only a single excitation peak with a maximum at 512 nm similar to wtYFP (92). The midpoint redox potential $E^{\circ\prime}$ of rxYFP was

determined as −261 mV through redox titration of recombinant protein with 2GSH/GSSG buffers (92). Since the reactivity of rxYFP with glutathione is rather low, protein samples had to equilibrate for 21 hours and thus the adjusted 2GSH/GSSG mixture had to be carefully controlled for air oxidation of GSH.

Although fluorescence quenching of the neutral form of the chromophore in rxYFP would argue for exclusive usability of rxYFP as a single excitation wavelength probe only, Maulucci and colleagues report the use of rxYFP as a ratiometric probe (76). When expressed in human cells, the redox-dependent change in emission after excitation at 458 nm was only ~50% of the change observed after excitation at 488 nm. This difference was used for ratiometric calculations (60, 76, 77). However, it is not entirely clear if this kind of ratiometry can separate variations in probe concentration from changes in redox state. The exact excitation spectra for reduced and oxidized rxYFP inside cells are not known. Because the reference wavelength (458 nm) is close to the isosbestic point of YFP, the fluorescence excited is very low and thus may be significantly obscured by background noise, which needs to be subtracted very carefully. This already implies that such analysis of rxYFP might be very sensitive to autofluorescence. Furthermore, the fact that the redox-dependent change in fluorescence points in the same direction for both excitation wavelengths inevitably lowers the dynamic range of the probe. Another issue that may be relevant for the interpretation of measurements is the sensitivity of YFP to changes in pH at near neutral conditions with a chromophore pK_a of 7.0 (30) and the significant sensitivity of YFP to chloride (62,125).

2. roGFPs. The limitations due to lack of ratiometric properties were overcome with the development of redox-sensitive GFPs (roGFPs) (49). Starting from either wtGFP or EGFP, respectively, two cysteines were engineered into the positions S147 and Q204, which are located on β-strands 7 and 10 in close proximity to the positions mutated in rxYFP. The resulting redox probes were called roGFP1, which is based on wtGFP, and roGFP2, which is derived from EGFP. The two excitation maxima characteristic of GFP (~400 nm for the A-band and 475–490 nm for the B-band) are maintained in the respective roGFP variants with band A being the main excitation peak in roGFP1 and band B dominating in roGFP2. Oxidation results in an increase in the A-band and a decrease in the B-band and an inverse behavior under reducing conditions, as shown exemplarily for roGFP2 in Figure 2. For both probes a clean isosbestic point at ~425 nm was identified. With these spectral characteristics both roGFPs are *bona fide* ratiometric sensors.

RoGFP2 has been crystallized in both the reduced and oxidized states (PDB entries 1JC0 and 1JC1) (49). A comparison between the two structures highlights structural changes that likely explain the disulfide-induced shift in chromophore protonation. Formation of the disulfide bridge shifts one β-strand relative to the other and this causes several small structural rearrangements. Significant movements involve H148 (neighbor of C147 on strand 7) and S205 (neighbor of C204 on strand 10) (Fig. 3). H148 is located in H-bonding distance to the phenolic oxygen of Y66 and moves slightly away from the chromophore upon disulfide formation. The OH group of S205 (part of the ESPT hydrogen bonding network) moves relative to the water molecule and the E222

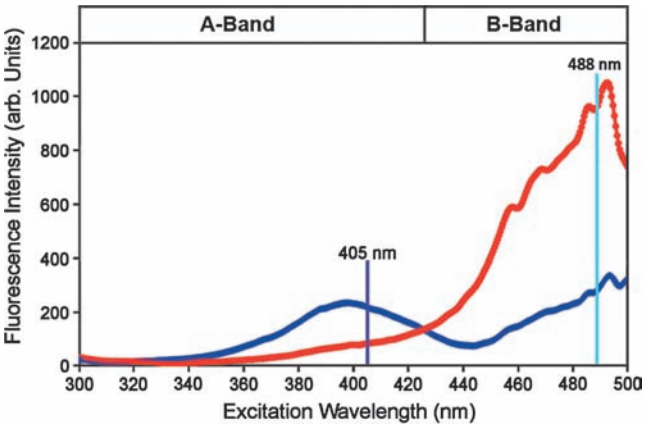

FIG. 2. Redox-dependent changes in the excitation spectrum of roGFP2. Because of the S65T mutation, the chromophore of reduced roGFP2 is preferentially deprotonated, thus exhibiting a predominant excitation maximum around 488 nm (*red curve*). Upon oxidation, the chromophore of roGFP2 is preferentially protonated, thus gaining excitability at 405 nm and loosing excitability at 488 nm (*blue curve*). (For interpretation of the references to color in this figure legend, the reader is referred to the web version of this article at www.liebertonline.com/ars).

carboxylate. It appears likely that these changes influence the Y66 protonation state and thus explain the ratiometric shift in the excitation spectrum.

Midpoint redox potentials for roGFPs have been determined through titration with DTT, lipoic acid, or bis(2-mercaptoethyl) sulfone (BMES) (27, 49). Generally, the determined midpoint potentials of −288 to −294 mV for roGFP1 and −272 to −287 mV for roGFP2 are more negative than the midpoint potential of rxYFP. Although the use of different redox buffers for titration led to slightly different apparent midpoint potentials, the ranking of roGFP1 as more reducing than roGFP2 was found to be preserved (27). For future applications, Dooley and colleagues suggested consensus midpoint potentials of −291 mV for roGFP1 and −280 mV for roGFP2 (27). A more precise determination of $E^{\circ\prime}$ for redox-sensitive FPs requires exact knowledge of the midpoint potential of the calibrating redox couple and avoidance of impurities in reduced and oxidized compounds.

In addition to the difference in midpoint potential, roGFP1 and roGFP2 also show some differences in their maximum achievable dynamic range for the change in fluorescence between fully reduced and oxidized probes (Table 1). If roGFPs are used as a single wavelength probe, they exhibit approximately a 3-fold change in fluorescence, which is only slightly better than the 2.2-fold change for rxYFP. However, because roGFPs are ratiometric, their dynamic range is significantly increased. With fully flexible filter-based detection systems such as epifluorescence microscopes or fluorescence plate readers, the probes can be excited exactly on the two excitation peaks, which would provide the largest achievable dynamic range. With excitation at 390 ± 5 nm and 480 ± 5 nm, roGFP2 has a dynamic range of about 12 (81). On appliances that use fixed wavelength lasers for fluorescence excitation such as confocal microscopes or fluorescence-activated cell sorting (FACS), the dynamic range is significantly lower due to

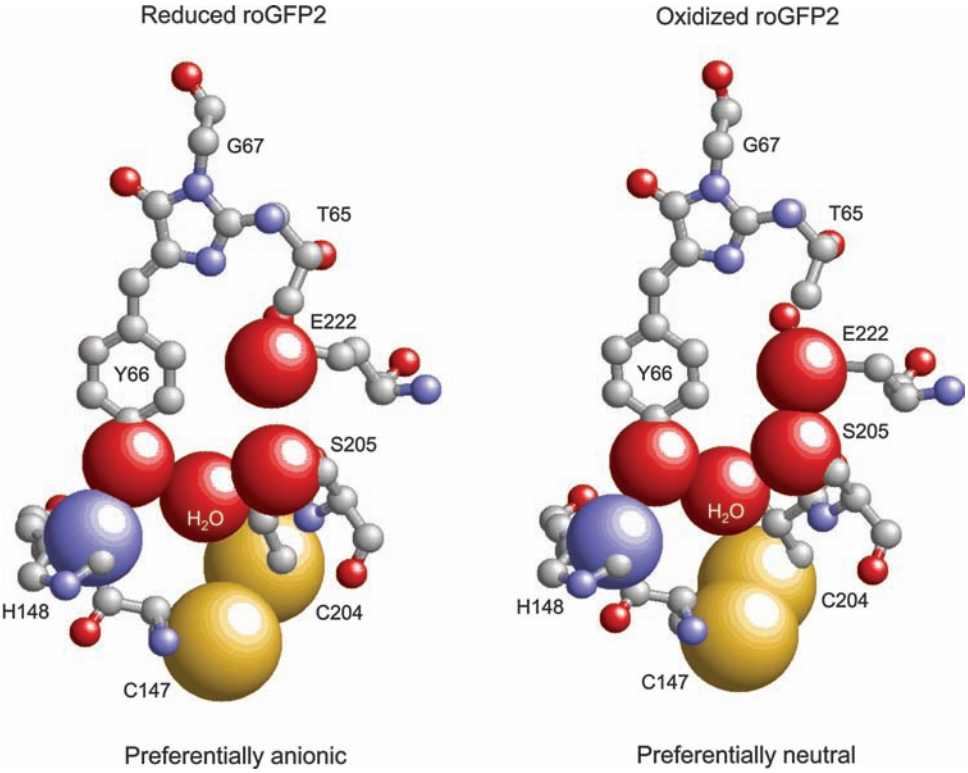

FIG. 3. Disulfide bond formation influences roGFP2 chromophore protonation. Upon formation of the C147–C204 disulfide bond, neighboring residues H148 and S205 are slightly shifted relative to the chromophore. H148 is in H-bonding distance to the phenolic oxygen of the chromophore. S205 is part of the hydrogen bonding network involved in proton transfer between the chromophore and E222. The figure is based on PDB entries 1JC0 (reduced roGFP2) and 1JC1 (oxidized roGFP2). Important atoms are shown as Van-der-Waals spheres: $S\gamma$(C147), $S\gamma$(C204), $N\delta1$(H148), O(Y66), $O\gamma$(S205), $O\varepsilon1$(E222), and O(H_2O). (For interpretation of the references to color in this figure legend, the reader is referred to the web version of this article at www.liebertonline.com/ars).

Table 1. Mutations and Redox Potentials of Disulfide-Based Redox Probes Derived from GFP

Redox probe[a]	*Engineered amino acids*	*Disulfide bond*	*Standard midpoint potential E°′ (mV)*	*Dynamic range*[b]
rxYFP[c]	S65A C48V Q80R N149C M153V S202C T203Y D234H	C149-C202	−261 (2GSH/GSSG)	2.2
rxYFP$^{200R/204R/227R}$ [d]	S65A C48V Q80R N149C M153V Y200R S202C Q204R T203Y A227R D234H	C149-C202	N.D.	N.D.
roGFP1[e,f]	C48S Q80R S147C Q204C	C147-C204	−288 (DTT_{red}/DTT_{ox}) −294 ($BMES_{red}/BMES_{ox}$) −291 (consensus)	2.58 (405/488)[i] 6.1 (400/475)[e]
roGFP2 [e,f]	C48S S65T Q80R S147C Q204C	C147-C204	−272 (DTT_{red}/DTT_{ox}) −287 ($BMES_{red}/BMES_{ox}$) −280 (consensus)	9.23 (405/488)[i] 5.8 (400/490)[e]
roGFP3[e]	C48S Q80R N149C S202C	C149-C202	−299 (DTT_{red}/DTT_{ox})	4.3 (400/475)[e]
roGFP4[e]	C48S S65T Q80R N149C S202C	C149-C202	−286 (DTT_{red}/DTT_{ox})	2.6 (400/490)[e]
roGFP1-R12[g]	C48S Q80R S147C N149K S202K Q204C F223R	C147-C204	−265 (DTT_{red}/DTT_{ox})	5.6 (400/475)[g]
roGFP1-iL[h]	C48S Q80R S147CL H148S Q204C	C147-C204	−229 (Dhl/La)	7.2 (400/475)[h]
roGFP1-iE[h]	C48S Q80R S147CE H148S Q204C	C147-C204	−236 (Dhl/La)	4.5 (400/475)[h]

[a]The table does not include all variants generated so far, but rather a selection considered most useful for biological applications.
[b]Dynamic range determined with the excitation wavelengths given in parenthesis.
[c]Ostergaard *et al*. (92).
[d]Hansen *et al*. (47).
[e]Hanson *et al*. (49).
[f]Dooley *et al*. (27).
[g]Cannon and Remington (13).
[h]Lohman and Remington (67).
[i]Schwarzländer *et al*. (107).
N.D., Not determined.

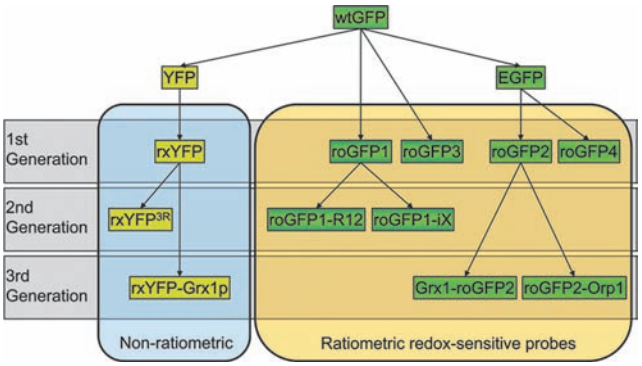

FIG. 4. Genealogy of genetically engineered fluorescent proteins with redox-sensitive disulfides. rxYFP^{3R} refers to the mutant rxYFP$^{200R/204R/227R}$. For further details and references, see text. (For interpretation of the references to color in this figure legend, the reader is referred to the web version of this article at www.liebertonline.com/ars).

off-peak excitation. The canonical laser wavelengths used for excitation of GFP are 405 and 488 nm. While the S65T mutation in roGFP2 shifts the excitation peak B for the anionic form of the chromophore to 490 nm, the anionic form of roGFP1 is excited with a maximum at 475 nm. When excited at 488 nm the dynamic range of roGFP1 is thus below 3, while roGFP2 would provide a theoretical dynamic range of ~9 (107).

3. Variants of rxYFP and roGFPs with altered properties. To match different needs and applications, it would be desirable to obtain a collection of probes with different midpoint potentials. For instance, to detect deflections from the steady state in both directions, probes with a midpoint potential matching the steady state redox potential of the environment under study are most appropriate. Along these lines, in addition to roGFP1 and roGFP2, four other variants, roGFP3 to roGFP6, have been engineered (Fig. 4; Table 1) (49).

RoGFP3 and roGFP4 differ from their siblings roGFP1 and roGFP2 in that they contain the disulfide bridge in position C149/C204. RoGFP5 and roGFP6 contain all four cysteines and thus can potentially form two internal disulfide bridges. However, none of these variants have been investigated in much detail so far and the presence of two disulfide bridges may render quantitative interpretation of the measured fluorescence ratio rather difficult. The variants roGFP3 and roGFP4, however, may have some potential for future applications. Although the observed dynamic range of theses variants is lower than that observed for roGFP1 and roGFP2, the midpoint potentials are slightly more negative. This is particularly true for roGFP3, which is derived from wtGFP, with the most negative midpoint potential of all roGFPs at −299 mV (49). Thus, in highly reducing compartments roGFP3 may have some potential for achieving more accurate measurements compared to other roGFPs.

The first generation of redox-sensitive FPs (rxYFP, roGFPs1-6) all had midpoint redox potentials of −260 mV or below, which made them most useful in reducing compartments, such as the cytosol, the mitochondrial matrix and chloroplast stroma (Table 1) (49, 92).

In the lumen of the endoplasmic reticulum (ER), rxYFP, roGFP1, and roGFP2 were fully oxidized, suggesting a redox potential higher than −240 mV (2, 49, 93). Thus, in oxidizing compartments the use of these probes is limited by their rather low midpoint potential. Recently, Lohman and Remington developed a new subfamily of roGFP variants derived from roGFP1, called roGFP1-iX, where 'X' denominates the insertion of different single amino acids into β-strand 7, adjacent to C147 (Fig. 4) (67). In conjunction with the exchange H148S the insertion resulted in an increased geometric strain in the disulfide, which renders the midpoint potential for the disulfide bond less negative. The least negative values were achieved with the insertion of leucine (−229 mV) and glutamate (−236 mV) (Table 1). Despite the very significant shift in $E^{\circ\prime}$, it is not yet clear whether an $E^{\circ\prime}$ of −230 mV is already sufficient for dynamic measurements in the ER.

To be reactive, thiols need to be de-protonated. The pK_a values of the two cysteines in rxYFP and roGFPs are all located between 8.9 and 9.5 (47, 49), which results in mostly protonated thiols and hence low reactivity. Introduction of basic amino acids next to cysteines can lead to stabilization of the thiolate form and thus was expected to increase the reactivity of the thiols in a series of 2nd generation redox-sensitive FPs (Fig. 4). Insertion of two lysines close to the two cysteines plus an arginine in position 223 led to a 6-fold increased rate constant in roGFP1-R12 (13). The insertion of up to three positive charges near the disulfide in rxYFP (rxYFP$^{200R/204R/227R}$) led to a 13-fold rate enhancement for the oxidation of rxYFP by GSSG (47). However, the achieved rate enhancements appear negligible for reactions *in vivo*, where the kinetic properties of redox-sensitive FPs are mainly determined through interaction with glutaredoxins (Grxs) (see Section III.A).

4. Interaction of rxYFP and roGFP with cellular redox pairs. When expressed in HeLa cells, the effective concentration for H_2O_2-induced oxidation of roGFPs was much lower than the concentration required *in vitro* (27). This observation suggested that oxidation of roGFPs inside cells is a catalyzed process. A link between roGFP oxidation and the cellular glutathione pool was indicated by a slight oxidation of roGFP in HeLa cells after a 2-hour incubation with 100 μM L-buthionine (*S,R*)-sulfoximine (BSO), a highly specific inhibitor of GSH biosynthesis. Furthermore, BSO-treatment also led to a highly increased sensitivity of roGFP to exogenously applied H_2O_2 (27).

At the same time, Jakob Winther and co-workers reported that rxYFP in yeast cells senses the glutathione redox potential (E_{GSH}) through interaction with Grxs (93). Thioredoxins, in contrast, were not capable of reducing or oxidizing rxYFP. A sensitive response of roGFP2 to depletion of cytosolic glutathione was shown in neuronal cells (121) and detailed studies in *Arabidopsis thaliana* confirmed that roGFP2, like rxYFP, is a quantitative biosensor for E_{GSH} (81). Expression of roGFP2 in the partially GSH-deficient *Arabidopsis* mutant *cad2*, which is restricted in the activity of the first and rate-limiting GSH biosynthetic enzyme glutamate-cysteine ligase (GSH1) (21), resulted in an increased 405/488 nm fluorescence ratio reflecting a shift in E_{GSH} towards less reducing values (Figs. 5B and 5C) (81). The detected shift in E_{GSH} closely matched expectations based on only 30% remaining glutathione and the assumption of constant glutathione reductase (GR) activity. In a more severe GSH1 mutant, *rml1*, which contains less than 5% of wild-type GSH (12,120), roGFP2 was almost completely oxidized (Fig. 5D). Taken together, studies

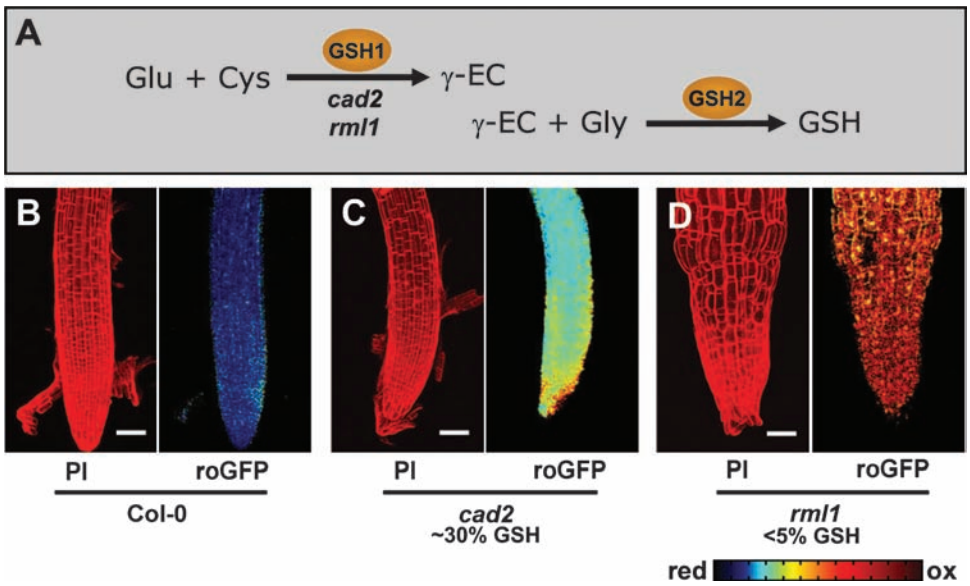

FIG. 5. Expression and ratiometric analysis of roGFP2 in *Arabidopsis*. (**A**) Biosynthetic pathway for GSH consisting of two enzymatic steps catalyzed by glutamate-cysteine ligase (GSH1) and glutathione synthase (GSH2). *cad2* and *rml1* are two partially GSH-deficient *GSH1* mutants. (**B–D**) Ratiometric analysis of roGFP2 in root tips of wild-type (Col-0), *cad2,* and *rml1* mutants indicates increasing oxidation of roGFP2 with deceasing GSH content. Propidiumiodide (PI) in intact cells exclusively labels cell walls and was used as a viability indicator. Scale bars = 50 μm. (For interpretation of the references to color in this figure legend, the reader is referred to the web version of this article at www.liebertonline.com/ars).

on rxYFP and roGFP strongly support the notion that within cells these proteins communicate with the glutathione redox couple through mediation by endogenous Grxs.

Several other redox-active compounds like NADPH and ascorbate, as well as oxidoreductases, such as Trxs and protein disulfide isomerases (PDIs), have been tested for interaction with roGFP *in vitro*, but none of these significantly affected the redox status of roGFP (40, 81) (Meyer *et al.*, unpublished results). However, given the broad spectrum of oxidoreductases in the Trx superfamily and other thiol-reactive proteins in cells, it cannot be excluded that some of these proteins may be capable of interacting with roGFP. As long as the Grx-catalyzed equilibration of roGFP with 2GSH/GSSG is kinetically favored, all such theoretically possible side reactions of roGFP should be overruled and high specificity of roGFP for E_{GSH} guaranteed. Translational fusion of an appropriate Grx to roGFP is a potent strategy to ensure constant kinetic coupling and fully reproducible probe specificity (see Section III.A).

5. The Nernst equation and its implications for using roGFPs. Based on the very well supported notion that roGFPs predominantly, if not exclusively, equilibrate with the 2GSH/GSSG redox couple, the redox behavior of roGFPs can be described and predicted by the Nernst equation, with various implications for the practical use of the probe. How fast the equilibrium is reached, or if it is reached at all, depends on the availability of Grx, which may differ between experimental systems. As discussed later on, the translational fusion of Grx to roGFP is a suitable strategy to ensure real-time equilibration (see Section III). The following calculations exemplarily apply to roGFP2.

a. Thermodynamics of roGFP2. Mathematically, the Grx-mediated exchange of electrons between glutathione and roGFP2 can be described by the Nernst equilibrium $E_{GSH} = E_{roGFP2}$, specifically

$$\begin{aligned} E_{GSH} &= E'^{\circ}_{GSH} - \frac{RT}{2F}\ln\left(\frac{[GSH]^2}{[GSSG]}\right) \\ &= E'^{\circ}_{roGFP2} - \frac{RT}{2F}\ln\left(\frac{[roGFP2_{red}]}{[roGFP2_{ox}]}\right) \\ &= E_{roGFP2} \end{aligned}$$

In this equation, R is the gas constant (8.315 J K^{-1} mol^{-1}), T the absolute temperature (298.15 K), and F the Faraday constant (96,485 C mol^{-1}). E'°_{GSH} is −240 mV (103) and E'°_{roGFP2} has been determined as −280 mV (27). For practical purposes, it is expedient to define the degree of oxidation (OxD) of the two interacting redox pairs:

$$OxD_{GSH} = \frac{2[GSSG]}{[GSH]+2[GSSG]} = \frac{2[GSSG]}{GSH_{total}}$$
$$OxD_{roGFP2} = \frac{[roGFP2_{ox}]}{[roGFP2_{ox}]+[roGFP2_{red}]}$$

Here, it is important to realize the definition for OxD_{GSH}. The total concentration of glutathione (GSH_{total}) refers to GSH equivalents (*i.e.*, $GSH_{total} = [GSH] + 2[GSSG]$). OxD_{GSH} is the fraction of GSH_{total} that exists as [GSSG]. For example, $OxD_{GSH} = 0.5$ does not mean that GSSG and GSH are in a 1:1 molar ratio, it rather means that 50% of all GSH equivalents exist as GSSG (*i.e.*, that GSSG and GSH are in a 1:2 molar ratio). As GSH_{total} is an important variable in biological settings, it is useful to express the Nernst equilibrium relationship as a function of OxD_{GSH}, GSH_{total} and OxD_{roGFP2}:

$$\begin{aligned} E_{GSH} &= E'^{\circ}_{GSH} - \frac{RT}{2F}\ln\left(\frac{2GSH_{total}(1-OxD_{GSH})^2}{OxD_{GSH}}\right) \\ &= E'^{\circ}_{roGFP2} - \frac{RT}{2F}\ln\left(\frac{1-OxD_{roGFP2}}{OxD_{roGFP2}}\right) = E_{roGFP2} \end{aligned}$$

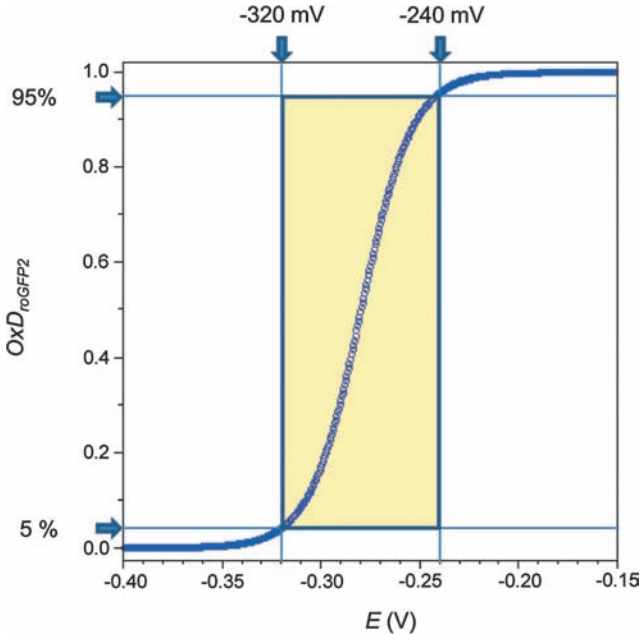

FIG. 6. Relationship between the redox potential (*E*) and the degree of sensor oxidation (OxD_{roGFP2}). Changes in probe fluorescence can be resolved in the window between 5% and 95% probe oxidation, which translates to an effective measuring range from −320 to −240 mV. (For interpretation of the references to color in this figure legend, the reader is referred to the web version of this article at www.liebertonline.com/ars).

This relationship allows to make various predictions and estimations about the behavior of the roGFP2-based biosensor system (see following sections).

b. Measuring range and calibration of roGFP2. The relationship between OxD_{roGFP2} and the redox potential E can be derived from the right half of the preceding equation:

$$OxD_{roGFP2} = \left(e^{\frac{2F\left(-E+E^{o'}_{roGFP2}\right)}{RT}}+1\right)^{-1}$$

This relationship reveals that the response of the probe becomes increasingly nonlinear when approaching 5% and 95% oxidation, respectively, and thus renders the detected signal sensitive to background noise (Fig. 6). For practical purposes, changes below 5% and above 95% sensor oxidation cannot be sufficiently resolved in fluorescence measurements. At best, roGFP2 can be expected to measure changes in E_{GSH} in the 80 mV-wide window between −320 and −240 mV (Fig. 6).

Suitably, the cytosolic E_{GSH} of unstressed cells is typically found in the range between −320 to −300 mV, close to the lower end of the practical measuring range. The measuring range of roGFP2 is well suited for measuring E_{GSH} in the cytosol and several other compartments, including the nucleus, mitochondria, and plastids. It is, however, not suitable for the ER, where it is oxidized at all times (81).

Given the available measuring range, is it feasible to derive absolute E_{GSH} values from fluorescence data? Of course, it would be highly desirable to calibrate intracellular measurements of E_{GSH} against independently confirmed standards. This, however, would require an independent compartment-specific approach to determine intracellular E_{GSH}. Unfortunately, no such alternative method is available. Since absolute intracellular calibration is not feasible, a more indirect way of calibration has to be performed. In a practical approach, to estimate intracellular E_{GSH} from the measured fluorescence ratio (R), externally applied cell-permeable reagents (typically dithiothreitol and diamide or H_2O_2) are used to deflect the probe *in situ* to the fully reduced and oxidized states. The resulting fluorescence ratios (R_{red} and R_{ox}) define the total range of the sensor inside intact cultured cells or transgenic tissues. Thus, the full set of measurements delivers six intensity values from which three ratios can be calculated (Table 2).

To establish a relationship between the macroscopic observables and OxD_{roGFP2}, several molecular quantities need to be defined: $i405_{red}$, $i405_{ox}$, $i488_{red}$, and $i488_{ox}$ are the fluorescence intensities contributed by a single roGFP2 molecule at the indicated wavelength and redox state, N_{total} is the total number of roGFP2 molecules, N_{red} is the number of reduced roGFP2 molecules, and N_{ox} is the number of oxidized roGFP2 molecules. Based on the assumption that the overall fluorescence intensity corresponds to the summation of fluorescence intensities from individual roGFP2 molecules, the relationships given in Table 3 apply.

By inserting the resulting equations (right column of Table 3) into $OxD_{roGFP2} = N_{ox}/N_{total}$, the relationship between OxD_{roGFP2} and the macroscopic observables can be deduced. As a result, OxD_{roGFP2} can be calculated directly from the six measured intensity values:

$$OxD_{roGFP2} = \frac{I405 \cdot I488_{red} - I405_{red} \cdot I488}{I405 \cdot I488_{red} - I405 \cdot I488_{ox} + I405_{ox} \cdot I488 - I405_{red} \cdot I488}$$

Or, alternatively, after transforming the same equation, using ratios:

$$OxD_{roGFP2} = \frac{R - R_{red}}{\frac{I488_{ox}}{I488_{red}}(R_{ox} - R) + (R - R_{red})}$$

In this equation, the quotient ($I488_{ox}/I488_{red}$) is most appropriately considered the 'instrument factor'. As the intensity at both wavelengths is linearly dependent on OxD_{roGFP2}, the

Table 2. Fluorescence Intensity Measurements Required for the Calculation of Redox Potentials

	Complete reduction (DTT)	*Complete oxidation (Diamide or H_2O_2)*	*Actual measurement*
Intensity at 405 nm	$I405_{red}$	$I405_{ox}$	$I405$
Intensity at 488 nm	$I488_{red}$	$I488_{ox}$	$I488$
Corresponding ratio	$R_{red} = \frac{I405_{red}}{I488_{red}}$	$R_{ox} = \frac{I405_{ox}}{I488_{ox}}$	$R = \frac{I405}{I488}$

Table 3. Relationships between Fluorescence Intensities and Probe Molecules

Limiting condition 1: Complete reduction	$N_{total} = N_{red}$ $N_{ox} = 0$	$I405_{red} = N_{tot} \cdot i405_{red}$ $I488_{red} = N_{tot} \cdot i488_{red}$
Limiting condition 2: Complete oxidation	$N_{total} = N_{ox}$ $N_{red} = 0$	$I405_{ox} = N_{tot} \cdot i405_{ox}$ $I488_{ox} = N_{tot} \cdot i488_{ox}$
Actual measurement	$N_{total} = N_{red} + N_{ox}$	$I405 = N_{ox} \cdot i405_{ox} + N_{red} \cdot i405_{red}$ $I488 = N_{ox} \cdot i488_{ox} + N_{red} \cdot i488_{red}$

ratio R is not (Fig. 7). Only in the special case that the isosbestic point (425 nm in the case of roGFP2) is used as the reference wavelength for ratiometry (instead of 405 nm) the instrument factor is canceling out from the equation, which then describes a linear relationship.

Having obtained OxD_{roGFP2}, the corresponding intracellular sensor redox potential E_{roGFP2} can be calculated from the Nernst equation:

$$E_{roGFP2} = E^{\circ'}_{roGFP2} - \frac{RT}{2F}\ln\left(\frac{1 - OxD_{roGFP2}}{OxD_{roGFP2}}\right)$$

Finally, assuming complete equilibration, E_{GSH} should equal E_{roGFP2}. Of course, the accuracy of the estimate is limited by measurement errors and differences in pH and temperature relative to the standard conditions. For a more detailed discussion of pH influence, see Section II.B.5.d below.

c. Sensitivity of roGFP2 towards changes in OxD_{GSH} *and [GSSG].* As the midpoint redox potential of roGFP2 (−280 mV) is much more negative than that of glutathione at physiological concentrations (ranging from −151 mV at 1 mM to −181 mV at 10 m*M*), even a small increase in the degree of glutathione oxidation will give rise to a large and disproportionate degree of sensor oxidation (Fig. 8). However, since E_{GSH} depends on GSH_{total}, so does the sensitivity of the probe towards changes in OxD_{GSH} and [GSSG].

It follows that roGFP2 should be a more sensitive indicator of OxD_{GSH} and [GSSG] in cells with low GSH_{total} as compared to cells with high GSH_{total}. Comparing overall cytosolic glutathione concentrations of 1 and 10 m*M*, broadly reflecting the variation between mammalian cell types, the difference in sensor oxidizablity is quite significant: At $GSH_{total} = 1$ m*M* 50% sensor oxidation is achieved with a 10-fold lower OxD_{GSH} (0.000088 vs. 0.00088) (Fig. 9A) and a 100-fold lower [GSSG] (44 nM vs. 4.4 μM) (Fig. 9B).

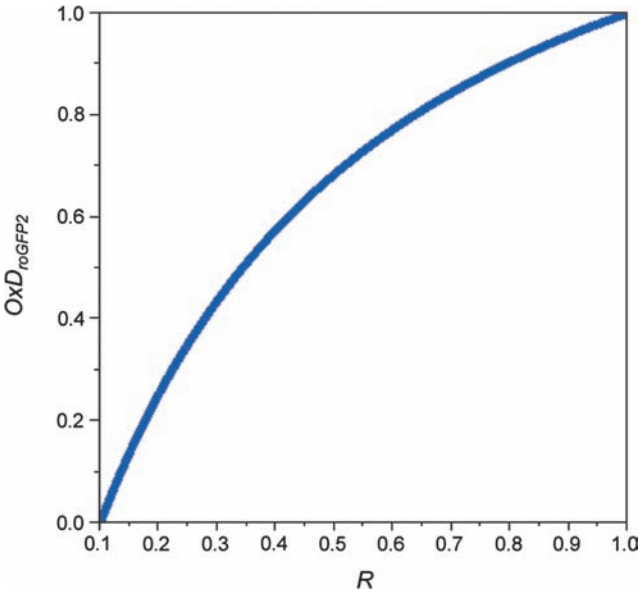

FIG. 7. The nonlinear relationship between OxD_{roGFP2} and the observed fluorescence intensity ratio *R*. *R* is the experimentally derived ratio of fluorescence intensities (*I*405/*I*488). In this graph the fully reduced probe corresponds to $R = 0.1$ and the fully oxidized probe to $R = 1$. (For interpretation of the references to color in this figure legend, the reader is referred to the web version of this article at www.liebertonline.com/ars).

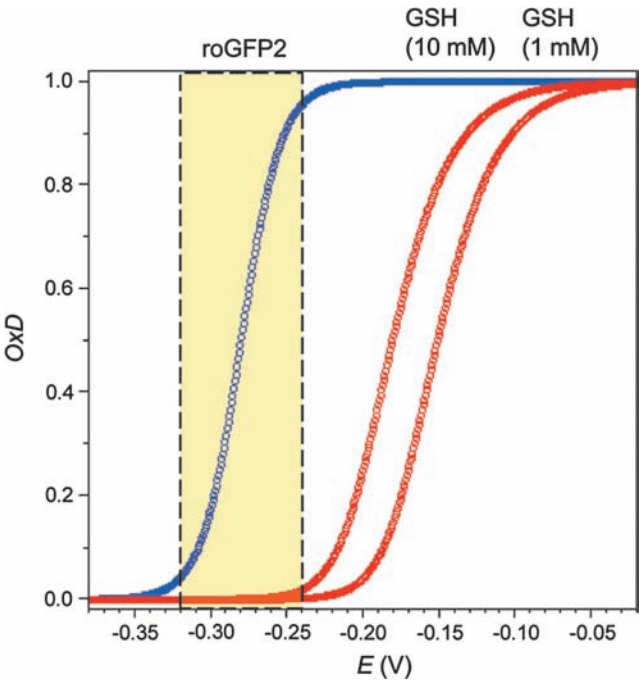

FIG. 8. Nernst relationship between the roGFP2 and glutathione redox couples. Comparison between roGFP2 (*blue curve*), glutathione at $GSH_{total} = 10$ m*M* (*left red curve*), and at $GSH_{total} = 1$ m*M* (*right red curve*). Within the measuring range of roGFP2 (*highlighted box*), small increases in the oxidation of glutathione lead to large increases in sensor oxidation. The difference in midpoint potentials ($E^{\circ'}_{roGFP2} - E^{\circ'}_{GSH}$) is inversely correlated to GSH_{total}. (For interpretation of the references to color in this figure legend, the reader is referred to the web version of this article at www.liebertonline.com/ars).

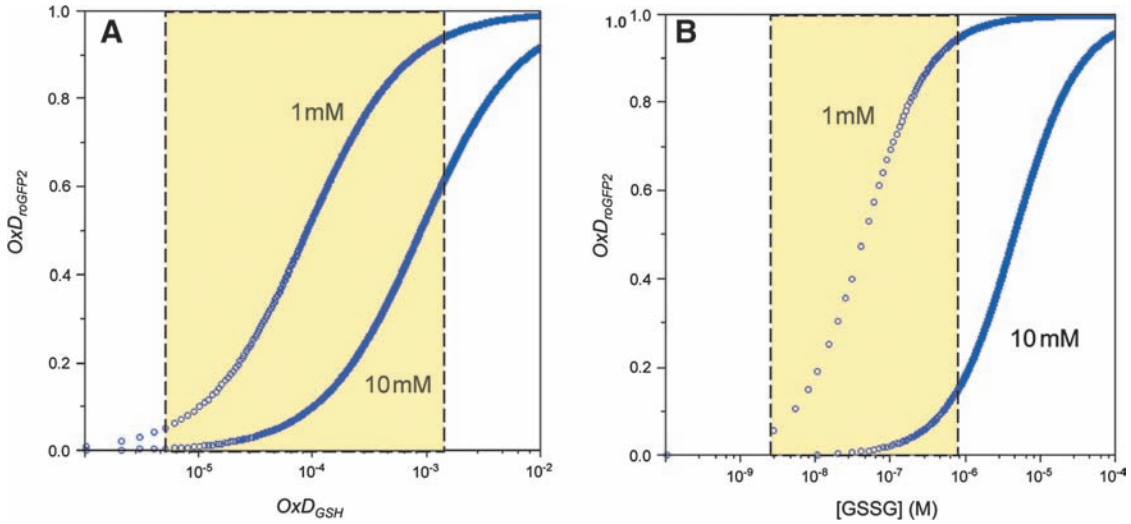

FIG. 9. Sensitivity of the roGFP2 response towards changes in OxD_{GSH} and [GSSG]. Comparison between 1 m*M* and 10 m*M* total glutathione concentration. (**A**) Relationship between OxD_{roGFP2} and OxD_{GSH}. (**B**) Relationship between OxD_{roGFP2} and [GSSG]. The measuring range of roGFP2 is highlighted for the curves representing $GSH_{total} = 1$ m*M*. (For interpretation of the references to color in this figure legend, the reader is referred to the web version of this article at www.liebertonline.com/ars).

To quantify the 'transmission' between glutathione oxidation and sensor oxidation—as afforded by the difference in midpoint potential between the two redox pairs—the OxD_{roGFP2}/OxD_{GSH} ratio at the sensor midpoint potential (−280 mV) can be considered. The 'transmission ratio' increases steeply with decreasing GSH_{total} and is 10-fold higher at 1 mM than at 10 mM (Fig. 10).

Although the 'transmission ratio' becomes very high with decreasing GSH, at $GSH_{total} = 10$ m*M* the 'transmission' is just sufficient to reliably observe changes in the lowest part of the physiological range between −320 and −300 mV. Specifically, at $GSH_{total} = 10$ m*M*, the shift of E_{GSH} from −320 to −300 mV corresponds to an absolute increase of [GSSG] from 200 to 930 n*M*, and a shift in OxD_{GSH} from 0.00004 to 0.00018. As a consequence, the oxidation of roGFP2 increases from 4% to 17%. If, however, a redox-sensitive FP with a midpoint potential of −260 mV had been used instead of roGFP2, it could not reliably 'perceive' this change at $GSH_{total} = 10$ m*M*, as its oxidation would just increase from 1 to 4%.

d. The influence of pH. How does pH influence the roGFP2 response? In principle, there are two ways by which pH can influence probes based on redox-sensitive FPs. Firstly, by influencing the fluorophore itself, and, secondly, by influencing the redox-sensing dithiol/disulfide pair. Direct influence on the fluorophore has been a concern, because the S65T mutation is expected to render roGFPs pH-sensitive. In fact, roGFP2 loses fluorescence at low pH, like other GFP variants with the S65T mutation (30). Fortunately, it turned out that pH-dependent fluorescence quenching affects both excitation wavelengths equally and that the calculation of excitation ratios effectively cancels out any pH effect in the range between 5.5 and 8.0 (107). The pH-insensitivity of the ratio was also confirmed for the fusion protein Grx1-roGFP2 (40), to be discussed later (see Section III.A.2).

What about the general influence of pH on thiol–disulfide equilibria? The reactivity of thiols and thus the redox potential is directly linked to the ambient pH because two protons are liberated during the formation of a disulfide bridge. As long as the pH does not approach the pK_a of the thiols forming the disulfide bond, the redox potential will change by approximately 59 mV per pH unit (103, 127). Consequently, a change in pH leads to a simultaneous change in E_{GSH} and E_{roGFP2}, into the same direction and by a very similar amount. Given a pK_a of 8.92 for glutathione (103) and assuming a pK_a of 9.0 for the

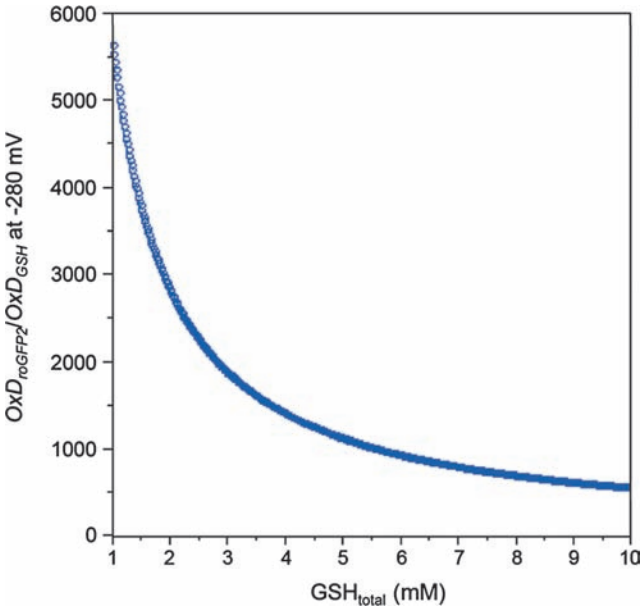

FIG. 10. The 'transmission ratio' OxD_{roGFP2}/OxD_{GSH} depends on the total concentration of glutathione. The ratio OxD_{roGFP2}/OxD_{GSH} is 560 at $GSH_{total} = 10$ m*M* and reaches 5700 at $GSH_{total} = 1$ m*M*. (For interpretation of the references to color in this figure legend, the reader is referred to the web version of this article at www.liebertonline.com/ars).

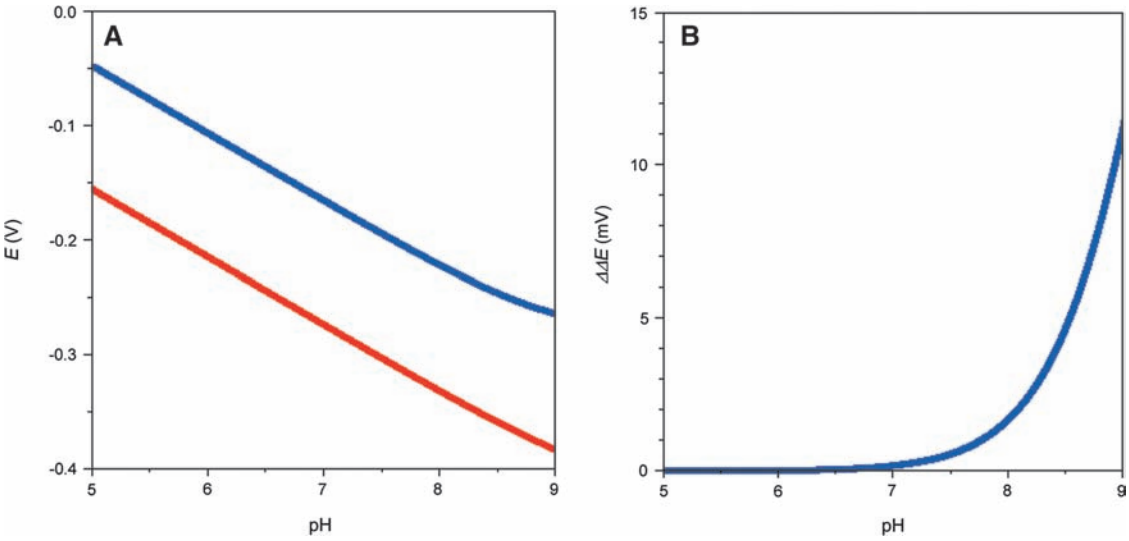

FIG. 11. Collinear pH-dependency of E_{roGFP2} and E_{GSH}. (**A**) The expected relationship between E and pH demonstrates collinearity for GSH (calculated for $pK_a = 8.92$ at $GSH_{total} = 5\,mM$, *blue curve*) and roGFP2 (for $pK_a = 9.0$, *red curve*). (**B**) Deviation from collinearity ($\Delta\Delta E$) becomes significant when the pK_a is approached, especially above pH 8. (For interpretation of the references to color in this figure legend, the reader is referred to the web version of this article at www.liebertonline.com/ars).

roGFP2 cysteines (14), it can be expected that the difference in redox potential between the two redox pairs is not significantly influenced by pH changes in the physiological range (Fig. 11A). The predicted deviation from co-linearity ($\Delta\Delta E$) amounts to just 2 mV at pH 8, but becomes more significant at higher pH (Fig. 11B).

This inference is supported by the *in vitro* observation that recombinant roGFP2 or Grx1-roGFP2 show the same response to GSH solutions adjusted to different pH in the range between 5.5 and 8.0 (Meyer *et al*., unpublished data; Gutscher *et al*., unpublished data). Thus, roGFP2 does not respond to pH-induced changes in E_{GSH} and should be regarded an indicator for pH-independent changes of E_{GSH}. It should be noted that pH nevertheless influences the kinetics of roGFP2-glutathione equilibration, which is faster at higher pH, attesting to the deprotonation of thiol groups involved in the exchange (Meyer *et al*., unpublished data; Gutscher *et al*., unpublished data). In conclusion, expressing roGFP2 in a compartment with different pH (*e.g.,* mitochondria) should not influence its sensitivity to oxidation by GSSG (compare Section II.B.5.c). However, if absolute mV values are to be estimated from fluorescence data, a correction for the assumed pH difference is required.

6. Applications of rxYFP and roGFPs. The applicability of conventional redox-sensitive FPs is limited by the kinetics of equilibration with the glutathione system (which may differ between species and cell types). As complete intracellular probe equilibration can take tens of minutes, conventional redox-sensitive FPs are best suited to determine steady state redox conditions and to document redox changes that are sufficiently long-lived to allow the probe to equilibrate.

a. Measurement of steady state redox conditions. RxYFP and roGFPs were originally developed to visualize the formation of disulfide bonds in living cells and to conduct noninvasive quantitation of thiol–disulfide equilibria in distinct subcellular compartments (49, 92). Expression of these probes in the cytosol of *Saccharomyces cerevisiae* (92, 93), HeLa cells (40, 49), airway epithelial cells (19, 106), pulmonary artery smooth muscle cells (19), human lung fibroblasts (59), *Arabidopsis thaliana,* and tobacco (8, 57, 81) consistently showed that the probe redox potential in the cytosol is close to or even below −300 mV. From these measurements it can be concluded that cytosolic [GSSG] is in the low-micromolar to mid-nanomolar range and thus several orders of magnitude lower than assumed before on the basis of conventional measurements in tissue extracts (81, 93). Consistent with this view, rxYFP-expressing yeast and roGFP-expressing plant mutants lacking cytosolic GR display an increased fluorescence ratio and a shift of 30 to 40 mV towards less negative E_{GSH} values (71, 93). Under severe oxidative stress the reducing function of GRs can be overruled. For example, treatment of *Drosophila* S2 cells with the redox cycling agent paraquat for 48–72 h led to severe oxidation of cytosolic roGFP (137).

The large overestimation of cytosolic [GSSG] by enzymatic or chromatographic analysis of cell lysates or tissue extracts likely results from the mixing of subcellular compartments and thus reflects the oxidized glutathione pool of the ER and, possibly, other organelles. In fact, all experiments in which redox-sensitive FPs have been targeted to the ER resulted in fully oxidized probes (49, 79, 81, 93). Oxidizing conditions in the ER lumen are generated though continuous formation of GSSG in oxidative protein folding (15). The ER membrane is considered to be impermeable to GSSG (64), thus keeping GSSG within the secretory pathway. In the absence of an ER-resident GR, it is thus not surprising that roGFP2 was found fully oxidized even in cell lines with defective oxidative protein folding (79). Of note, roGFP1 targeted to endosomes and lysosomes was also found to be oxidized, although these compartments have been expected to exhibit a reducing environment (2).

In mitochondria, chloroplasts and peroxisomes, roGFPs were found in the fully reduced state (49, 57, 106, 107). Despite

the local production of ROS in these compartments, cells are apparently capable of maintaining a high degree of glutathione reduction. For plants, it has been shown that GRs are present in all three types of organelles (18, 31, 101). Taking into account that the plant mitochondrial matrix and the chloroplast stroma are potentially alkaline with pH values up to 8 (10, 66), the estimated glutathione redox potentials in these compartments may be as low as −360 mV (49, 57, 106, 107).

b. Measurement of induced redox changes. Beyond the ability to target roGFPs to different subcellular compartments for steady state redox measurements, the biggest advantage of roGFPs over conventional fluorescent dyes is the reversibility of the oxidation reaction and thus the potential for recording dynamic redox changes in living cells.

All studies published to date have confirmed the dynamic response of intracellular roGFPs to exogenously applied oxidants and reductants. Typically, the reversibility of the cytosolic or mitochondrial roGFP response was demonstrated by sequential incubation with H_2O_2 and DTT (49, 57, 81, 106, 107) or aldrithiol (2,2-dipyridyl disulfide) and DTT (27, 43). Similar experiments have measured the time course of probe reduction following an exogenous oxidative challenge. However, interpretation of kinetic probe behavior is difficult, because the isoforms and concentrations of Grxs may differ between cell types and compartments. For example, following probe oxidation with exogenously applied H_2O_2, roGFP2 in *Arabidopsis* mitochondria recovered very slowly (108). This response pattern has been discussed to indicate prolonged endogenous ROS production induced by exogenous oxidative stress. It cannot be excluded though that the slow reduction of roGFP2 in plant mitochondria is caused by lack of appropriate Grxs for catalyzing equilibration between roGFP2 and the matrix glutathione buffer. Out of a large number of 31 Grxs in *Arabidopsis* (80), only two have been experimentally confirmed to be present in mitochondria (18, 51, 54). It is not known whether these Grxs are capable of interacting with roGFPs.

Other experiments have looked at the response of ER-localized roGFPs following an exogenously applied reductive challenge. RoGFP1 targeted to the ER lumen in airway epithelial cells was almost fully oxidized but could be reduced with 500 μM DTT (106). After washout of the reductant, the fully oxidized state was re-established within 7 min. The roGFP re-oxidation process was also investigated in yeast cells (79). After initial reduction of ER-resident roGFP2 by DTT, it was possible to compare the kinetics of re-oxidation in wild-type and mutant cells. Severely delayed oxidation of roGFP2 in a knockdown of Ero1p supports the view that Ero1p is the major net generator of disulfides in the ER lumen (11, 34, 109, 118).

Another category of intracellular redox changes, closer to physiological relevance, are those caused by endogenously produced oxidants. In a recent study, roGFP was used to investigate the effects of complex II inhibitors on mitochondrial ROS production (42). Acute administration of thenoyltrifluoroacetone (TTFA), an inhibitor of the ubiquinol binding site in complex II, resulted in a gradual increase in oxidation over a 30 min period. Oxidation induced by TTFA was significantly higher than that induced by inhibitors targeting the succinate binding site in complex II.

Time-resolved roGFP imaging was used to analyze hypoxia-induced ROS formation in mouse pulmonary artery smooth muscle cells (25). Within minutes from the onset of hypoxia, OxD_{roGFP} increased from ~12% to ~17%, a value that was maintained throughout the 30 min hypoxia treatment. After moving back to normoxic conditions, roGFP oxidation returned to base levels. The oxidation of roGFP during hypoxia was prevented by overexpression of catalase, implying a role for H_2O_2. A slight decrease in roGFP oxidation was observed during hypoxia in AML12 liver cells (43). It is, however, impossible to directly compare these observations because Desireddi *et al.* (25) present their data as % oxidation of roGFP, while Haga *et al*. (43) present the 400/480 nm fluorescence ratio. In addition, it is not clear whether the measurements are based on the same roGFP variant. As described in Section II.B, the fluorescence ratio and the achievable dynamic range depend on the roGFP variant and the excitation wavelengths employed. In contrast to the fast recovery of roGFP after return to normoxic conditions reported by Desireddi *et al*., Haga and colleagues found rapid oxidation immediately following re-oxygenation (43). Oxidation gradually increased over 60 min and was more pronounced after prolonged hypoxia. External application of *N*-acetylcysteine and catalase before onset of hypoxia prevented post-hypoxic roGFP oxidation. In the same study, adenovirally expressed roGFP was also used to monitor redox changes in the murine liver during ischemia and reperfusion. Similar to cell culture experiments, hepatic ischemia immediately led to increased roGFP reduction followed by a rapid partial oxidation within 5 min after ischemia ended (43).

c. roGFPs as topology reporters for membrane proteins. Current estimates indicate that 20%–30% of all predicted open reading frames in a typical genome code for transmembrane

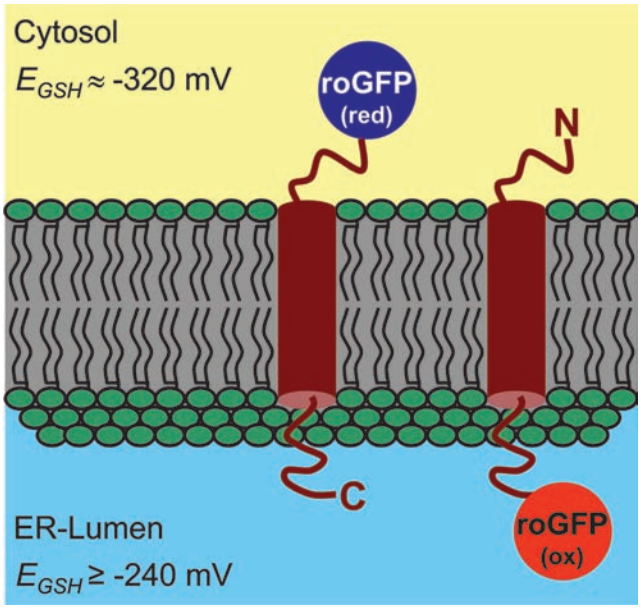

FIG. 12. The redox-based topology assay (ReTA) enables direct visualization of membrane protein topology. Ratiometric imaging of roGFP fused to membrane proteins either at their N- or C-termini provides a binary readout for the orientation of the roGFP tag relative to the membrane. (For interpretation of the references to color in this figure legend, the reader is referred to the web version of this article at www.liebertonline.com/ars).

(TM) proteins (122), but the number, location and orientation of transmembrane domains (TMDs), as predicted by bioinformatics algorithms are often highly contradictory (29). Despite the general biological importance of TM proteins, tools for experimental analysis of the protein topology are limited. In yeast, the topology of TM proteins can be investigated *in vivo* using fusions with essential metabolic enzymes as topology reporters and expression of these fusions in a mutant background (58). This approach, however, is not feasible for most other eukaryotic cell types because suitable mutants are often lacking. An advanced method to analyze the topology of TM proteins *in vivo* is the redox-based topology analysis (ReTA) in which roGFP2 is exploited as a topology reporter (8) (Fig. 12). The only requirement for ReTA to be applicable is a distinct gradient in E_{GSH} across the membrane the TM protein of interest is targeted to. Such a gradient exists across the ER membrane and thus all TM proteins passing through the ER are prime candidates for ReTA. The straightforward ratiometric analysis without the need of any calibration provides a binary readout for the orientation of the protein within the membrane (8). For further analysis of the entire protein topology, roGFP can be fused to truncated versions of the protein or the probe can be inserted into (putative) extra-membrane loops. The latter approach has been shown to be feasible by inserting conventional GFP into PIN5, an atypical member of the PIN auxin-efflux-carrier family in plants (88). Oxidized roGFP2 has a pK_a of 6 (49) and thus could be quenched to a large extent in acidic compartments such as lysosomes, plant vacuoles, and the apoplast in plants. Loss of fluorescence on one side of the membrane would impede binary ratiometric readouts. Since most proteins in these membranes pass through the ER and their topology is assumed not to change during passage through the secretory pathway, it may still be possible to analyze their topology by ReTA within the ER (8). Another possibility to overcome fluorescence quenching in acidic compartments may be to use the pH-insensitive roGFP1, which is assumed to have a much lower pK_a in the order of the apparent pK_a near 4.5 determined for wtGFP (117).

ReTA can be expanded to the analysis of protein orientation in nonsecretory membranes provided a sufficient E_{GSH} gradient is present. For mitochondria it has been shown that rxYFP is partially oxidized in the intermembrane space (IMS), whereas the probe was considerably more reduced in the cytosol and the mitochondrial matrix (56). Based on this finding, ReTA should also be applicable to mitochondrial membrane proteins. Applicability of ReTA to TM proteins of the chloroplast envelope in plants would also depend on the ability to measure E_{GSH} in the IMS of the chloroplast envelope. So far, however, no successful expression of any fluorescent protein has been reported for the plastidic IMS (*e.g.*, (5)). Nevertheless, it can be envisaged that the topology of TM proteins in the inner membrane can be investigated in a mutant background specifically affected in plastidic GSH levels and thus plastidic E_{GSH}. With these amendments ReTA is considered to be broadly applicable and the most simple-to-use method currently available for the analysis of TM protein topology in higher eukaryotic cells (8).

C. cpYFP as a putative probe for superoxide

$O_2^{\bullet-}$ is the primary ROS generated by the photosynthetic and respiratory electron transport chains, as well as the Nox enzymes. Localized generation of $O_2^{\bullet-}$ has been reported to accompany signaling and stress in both plants and animals (33, 63, 65). To understand the biological significance of such localized $O_2^{\bullet-}$ production and the dynamics of associated signaling cascades, it would be highly informative to specifically record the formation of $O_2^{\bullet-}$ as the first intermediate in such pathways. Rather unexpectedly, it was recently reported that cpYFP is capable of responding to $O_2^{\bullet-}$ (126). In cpYFP, the amino and carboxyl portions of YFP have been interchanged with a short connecting linker between the original termini, while the axial α-helix containing the chromophore maintained its central position in the β-barrel. CpYFP was originally generated to develop so-called Pericam probes, which are genetically encoded Ca^{2+} sensors (3, 89). The Ca^{2+}-sensing function was engineered into cpYFP by fusing the Ca^{2+}-binding protein calmodulin and its target peptide M13 to the novel N- and C-termini of cpYFP. CpYFP was first reported to have two excitation peaks at 417 and 506 nm, which is reminiscent of the bimodal excitation spectrum of wtGFP (89). In contrast, Wang and colleagues reported that their cpYFP exhibited only a single excitation maximum at 490 nm and an emission maximum at 515 nm (126). Instead of the second excitation peak at shorter wavelength (89), Wang *et al.* reported an isosbestic point near 405 nm excitation, permitting ratiometric measurement via dual wavelength excitation (488 nm/405 nm) (126).

When cpYFP was expressed in mitochondria, the probe apparently responded to $O_2^{\bullet-}$ produced by the respiratory chain (126). *In vitro*, cpYFP was found to be five times brighter under strong oxidizing conditions imposed by incubation with aldrithiol as compared to ambient redox potentials between −7.5 mV and −319 mV set by incubation with a DTT redox buffer. Furthermore, cpYFP seemed to respond to enzymatically synthesized $O_2^{\bullet-}$, but not to H_2O_2 and $ONOO^-$. Hydroxyl radicals and $NO^{\bullet}$ caused a slight decrease of fluorescence rather than an increase (126). Similarly, NADH did not cause a significant change in cpYFP fluorescence. The authors interpreted fluctuations in cpYFP fluorescence as quantal bursts of $O_2^{\bullet-}$ production ($O_2^{\bullet-}$ flashes) within the matrix of individual mitochondria in quiescent cells under resting conditions.

The correct interpretation of changes in cpYFP fluorescence depends on the understanding of the underlying chemistry. Unfortunately, at this stage there is no good explanation for $O_2^{\bullet-}$-induced changes of chromophore properties. In principle, $O_2^{\bullet-}$ can act as an oxidant or reductant. $O_2^{\bullet-}$ only rarely oxidizes biological compounds because the anionic charge limits reactivity with electron-rich centers (130). Nevertheless, Wang and colleagues considered the two residues C171 and C193 in the cpYFP molecule as potential targets of $O_2^{\bullet-}$ (126). Indeed mutation of both cysteines to either alanine or methionine abrogates the sensitivity to aldrithiol, but it also largely reduces fluorescence of the entire molecule. C171 and C193, which are in close proximity to the chromophore on the central α-helix spanning the β-barrel, are equivalent to C48 and C70 in the parental GFP molecule. Loss of fluorescence was also reported earlier for the single mutation of C70 in GFP. While mutation of C48 does not affect the fluorescence of GFP, substitution of C70 proved to be deleterious to obtaining soluble, fluorescent protein (49). This deleterious effect makes the interpretation of the double cysteine mutant of cpYFP partly ambiguous. For further characterization of cpYFP, it

would be necessary to study the properties of the respective single cysteine mutations.

While the interior of GFP is hardly accessible to small molecules, circular permutation of the protein results in obvious clefts in the β-barrel that may allow access for H^+ and other small molecules to the chromophore. Indeed, cpGFP is more sensitive to acidic pH than EGFP and is acid-quenched below pH 6 (3). A change in protonation of the chromophore, however, should be detectable at both excitation wavelengths with opposite direction. In the case of cpYFP, such an effect of pH on the chromophore appears unlikly because a change in fluorescence was only observed with excitation at 488 nm, but not with excitation at 405 nm (126). In conclusion, more detailed studies are required before cpYFP can be adopted as a probe for superoxide.

III. Redox Relays Based on Redox-Sensitive FPs

Most recently, chimeric fusion proteins of redox-active enzymes and redox-sensitive FPs have been explored for their use as redox probes. A redox enzyme may be coupled directly to redox-sensitive FPs by electron transfer, thus forming a redox relay. The rationale behind this approach is the idea that redox enzymes will lend specificity and efficiency to a redox sensing process. The investigation of this principle was motivated by the fact that conventional roGFPs did not show responses to weak transient oxidative processes as they occur in a physiological setting (*e.g.*, after growth factor stimulation) (27, 46). Since, on the other hand, roGFPs indicated pronounced redox differences between subcellular compartments (ER vs. cytosol), it was obvious that they nevertheless adjust to a steady state redox potential. Thus, it seemed that conventional roGFPs are limited by a slow response to oxidative changes (which may require tens of minutes) (13). As discussed, roGFPs are capable of equilibrating with 2GSH/GSSG, but in many situations this equilibration is too slow to allow the detection of transient and weak oxidative changes. Based on this consideration, it was hoped that the proximity of a covalently attached redox catalyst (present in a very high local concentration) in a 3rd generation of redox-sensitive FPs (Fig. 4) would facilitate rapid and complete equilibration with a defined cellular redox couple.

A. Coupling redox-sensitive FPs to glutaredoxins

1. rxYFP-Grx1p. Following the observation that rxYFP in yeast cells equilibrates with glutathione (93), the first investigation into the direction of fusion-based redox relays was done by the group of Jakob Winther. The fusion between rxYFP and yeast Grx1p (rxYFP-Grx1p) was primarily used as a biochemical tool to study the reaction mechanism of Grx. The fused Grx was found to operate through the monothiol mechanism. RxYFP oxidation was improved by a factor of 3300 and proceeded with almost absolute glutathione specificity (7). The crystal structure of rxYFP-Grx1p did not reveal direct contacts between the two protein domains, thus suggesting that it is the enhanced collision rate between the two domains that is responsible for the much improved thiol–disulfide exchange efficiency (44).

2. Grx1-roGFP2. As described in Section II.B.4, it had become clear that roGFPs, like rxYFP, interact with the glutathione system (81). This led to the question if Grx-based chimeric fusion proteins are suitable as redox probes for live imaging of redox changes in mammalian cells. To create a probe for E_{GSH}, human Grx1 and roGFP2 were chosen as fusion partners (40). RoGFP2 was considered to be the most suitable redox-sensitive FP for the purpose of developing a biosensor. As discussed before, a general advantage of roGFPs over rxYFP is that they are ratiometric by excitation, thus making measurements insensitive to differences in sensor concentration and photobleaching (49). In addition, the midpoint potential of roGFP2 (−280 mV) is more negative than that of rxYFP (−261 mV), thus making the roGFP2 response more sensitive to oxidation by small increases in glutathione oxidation (compare Section II.B.5.c). roGFP2 was preferred over roGFP1 (49), mainly for three reasons: (i) roGFP2 is brighter, (ii) its two excitation maxima better match standard laser lines (405 and 488 nm), and (iii) the S65T mutation makes roGFP2 resistant to photoswitching, which may create artifacts by shifting fluorescence ratios (107). Due to their limited dynamic range, roGFP3 and roGFP4 (49) were not considered for the purpose of biosensor development.

a. The general concept behind Grx1-roGFP2. The intracellular response of nonfused roGFP2 is limited by the availability of endogenous Grx, which appears to be insufficient for rapid equilibration in many systems and situations. This also means that differences in Grx abundance and activity between species, cell types, subcellular compartments and developmental or environmental situations will influence the kinetics of equilibration between roGFP2 and glutathione, making observations much less comparable and reliable. To solve the problem of slow and variable equilibration, roGFP2-fused Grx is exploited to enforce continuous equilibration between the two redox pairs $roGFP2_{red}/roGFP2_{ox}$ and 2GSH/GSSG.

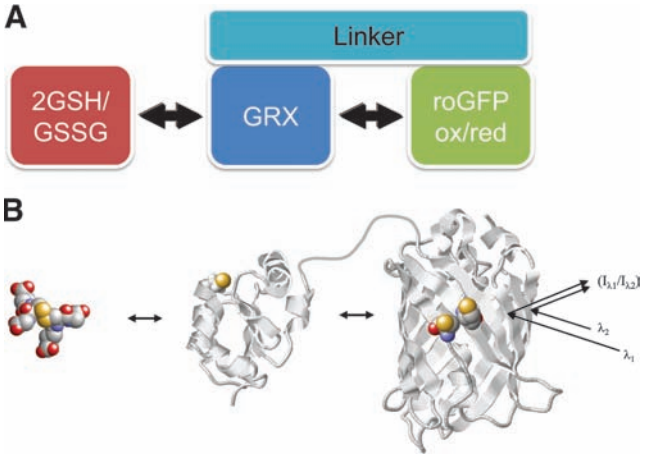

FIG. 13. Principle of the Grx1-roGFP2 redox biosensor. (**A**) RoGFP2-linked Grx efficiently catalyzes equilibration between glutathione and roGFP2. (**B**) Structural model showing glutathione disulfide and the Grx1–roGFP2 fusion protein in the reduced state. The redox state of roGFP2 is obtained by ratiometric fluorescence intensity (I) measurements at two different excitation wavelengths (λ_1, λ_2). (For interpretation of the references to color in this figure legend, the reader is referred to the web version of this article at www.liebertonline.com/ars).

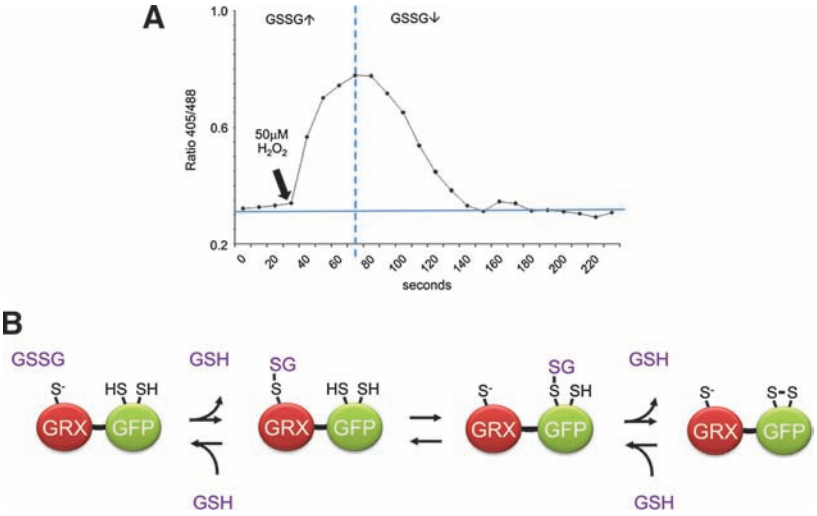

FIG. 14. Reversibility of the Grx1-roGFP2 response. (**A**) Live cell imaging of the intracellular Grx1–roGFP2 response to an oxidative challenge from outside the cell. H_2O_2 entering the cell is rapidly converted to GSSG (presumably by glutathione peroxidases), which then oxidizes the probe. Once H_2O_2 is depleted, GSSG levels drop (due to glutathione reductase) and the sensor re-equilibrates. (**B**) Molecular mechanism of the Grx1–roGFP2 biosensor. Each individual step of the three-step thiol-disulfide exchange cascade is fully reversible. (For interpretation of the references to color in this figure legend, the reader is referred to the web version of this article at www.liebertonline.com/ars).

By covalently attaching the redox catalyst to roGFP2, its local concentration is dramatically increased. For approximation, assuming that Grx1 is restricted by the linker to an operating range of ~75 Å, the local Grx1 concentration experienced by each roGFP2 molecule is ~1000 times higher (~1 m*M*) than the estimated absolute concentration of Grx1-roGFP2 in the cell (~1 μM). The local Grx1 concentration experienced by roGFP2 is thus also at least three orders of magnitude higher than the concentration of endogenous Grx1 distributed in the mammalian cytosol (37). By making Grx an integral part of the probe, the biosensor becomes catalytically self-sufficient in securing rapid and efficient equilibration under all circumstances (Fig. 13).

b. The molecular mechanism of Grx1-roGFP2. The response properties of Grx1-roGFP2 are based on the well established monothiol mechanism of Grxs (32, 98). This conclusion is supported by the finding that removal of the second active site thiol (C26) does not compromise the redox-sensing behavior of Grx1-roGFP2 *in vitro* or in live cell experiments (Gutscher *et al.*, unpublished results). Likewise, the monothiol mechanism has also been established for rxYFP-Grx1p (7). In the oxidative response, the nucleophilic cysteine C23 of Grx1 specifically reacts with GSSG to form a mixed Grx1-glutathione disulfide intermediate. The latter reacts with one of the two thiols on roGFP2, which, as a consequence, becomes *S*-glutathionylated. The existence of *S*-glutathionylated intermediates has been confirmed by mass spectrometry (Meyer *et al.*, unpublished data), but it remains unclear if one of the two roGFP2 cysteines is preferentially *S*-glutathionylated by Grx. In the last step, glutathionylated roGFP2 re-arranges to form the internal disulfide bridge (C147–C204). Importantly, the three consecutive steps of thiol–disulfide exchange are fully reversible. When an oxidative event fades away, [GSSG] and thus E_{GSH} rapidly normalize, and the whole three-step thiol–disulfide cascade re-equilibrates (Fig. 14A). Grx1-roGFP2 is a truly dynamic probe because it is based on a completely symmetrical ping-pong mechanism (Fig. 14B).

c. Specificity of Grx1-roGFP2. Grx1-roGFP2 is expected to have a very high specificity for the 2GSH/GSSG redox couple as interactions of the roGFP2 domain with other redox couples are less likely to occur in the omnipresence of fused Grx. Grx by itself is highly specific for the interaction with glutathione and this specificity was also confirmed for the rxYFP-Grx1p and Grx1-roGFP2 fusion proteins (7, 40). Importantly, roGFP2 is not capable of interacting with the Trx system (see below), a fact that also contributes to overall probe specificity. When using Grx1-roGFP2 to investigate intracellular redox changes, it is important to realize that it is a probe for E_{GSH}, no more and no less. As such, Grx1-roGFP2 will directly respond to changes in either OxD_{GSH} or GSH_{total} (with the exception of being mostly indifferent to pH-induced changes in OxD_{GSH}, see Section II.D). Shifts in OxD_{GSH} can be caused by several factors, including changes in $[H_2O_2]$, but not restricted to it. It must be kept in mind that the response of intracellular Grx1-roGFP2 to H_2O_2 is indirect. Although direct oxidation of roGFP2 thiols by H_2O_2 is thermodynamically favored, it is kinetically very slow. The pK_a of both thiols on roGFP2 is at least 9 (13) and without catalysis, thiols and H_2O_2 generally react very slowly (131). It is safe to assume that the response of Grx1-roGFP2 to physiological concentrations of H_2O_2 is always indirect in that H_2O_2 must first give rise to GSSG. Although it is expected that a rise in $[H_2O_2]$ will typically entail an increase in OxD_{GSH}, it should not be taken for granted to occur under all circumstances. For example, it is conceivable that under certain conditions H_2O_2 scavenging is dominated by peroxiredoxins and takes place without contribution by glutathione peroxidases. In this case, OxD_{GSH} would not be significantly affected by H_2O_2.

d. Reliability of Grx1-roGFP2. Given the operating mode of Grx1-roGFP2, can we think of intracellular conditions that may compromise sensor function or even lead to false results? One possible concern is that the activity of the Grx1 domain could be subject to modulation by post-translational modification. Although there is no evidence for phosphorylation or other modifications, it should be noted that wild-type human Grx1 harbors three additional cysteines that are not essential for activity (C8, C79, and C83). It has been reported that oxidative modifications of these residues can negatively influence Grx activity *in vitro* (50), albeit the study used rather nonphysiological conditions and the *in vivo* relevance of this

finding remains unclear. A roGFP2 fusion protein based on a Grx1 mutant lacking all three extra cysteines did not show a difference in redox behavior, neither *in vitro* nor inside cells (Gutscher *et al.*, unpublished data). Thus, at present there are no indications that the Grx1-roGFP2 response is influenced by the Grx1 extra cysteines. However, to avoid uncertainties, it may be preferable to use modified versions of Grx1-roGFP2 lacking C8, C79 and C83.

Whenever a genetically encoded probe is (over)expressed in cells, there is a possibility of perturbation, especially if the probe is based on an enzyme. Is it conceivable that Grx1-roGFP2 disturbs intracellular E_{GSH}, thus distorting its own measurements? This scenario appears unlikely. On the one hand, the reducing equivalents (thiols) introduced by the probe are negligible relative to the overall glutathione and protein thiol pools, both in the millimolar range (48). On the other hand, Grx1 is not known to create or destroy oxidizing equivalents and the redistribution of disulfide bonds catalyzed by Grx1 is not expected to alter E_{GSH}. In fact, when roGFP2- and Grx1-roGFP2-expressing cells were compared, their steady state E_{GSH} was not significantly different (Gutscher *et al.*, unpublished data), strengthening the notion that the additional Grx1 brought into the cell by the fusion protein does not influence E_{GSH}.

Another question though is if the additional Grx1 could influence other aspects of cellular behavior, for example, by impacting signaling. In mammalian cells, endogenous Grx1 has been found to be associated with ASK1 and procaspase-3 and may have a role in regulating these proteins (96, 112). Although it may be argued that fused Grx1 is poised to act on its fusion partner roGFP2, it cannot be excluded that roGFP2-linked Grx1 catalyzes glutathionylation/deglutathionylation of other proteins as well. Overexpression of Grx1-roGFP2 in HeLa cells did not influence proliferation rate or sensitivity to apoptosis relative to nontransfected cells (Gutscher *et al.*, unpublished data). Nevertheless, as with other genetically encoded probes, the principal possibility of changing some aspects of cell physiology must be kept in mind. To minimize the potential risk of unwanted Grx interactions, it seems reasonable to use a distantly related Grx, for example, bacterial Grx for E_{GSH} measurements in human cells. However, the performance of such alternative E_{GSH} probes remains to be tested.

Finally, the structural integrity of GFP chimeric proteins is another general issue as proteolytic fragments may compromise the overall sensor response. In some cases, the linker must be optimized to minimize folding interference and proteolysis. When expressed in HeLa cells Grx1-roGFP2 did not show signs of degradation despite its rather long linker of 30 amino acids (Gutscher *et al.*, unpublished data).

e. Sensitivity of Grx1-roGFP2. As discussed before, in addition to improved specificity, the major advantage of Grx1-roGFP2 is its rapid equilibration with the glutathione redox pair independently of endogenous Grx availability. Grx1-roGFP2 has been used to visualize changes in E_{GSH} with minute resolution, as they occur during mitochondrial depolarization and receptor crosslinking (40). Rapid equilibration makes Grx1-roGFP2 responsive to oxidative events that are short-lived and weak, and it is these events that are easily missed by conventional roGFP2. As discussed before, no independent method for compartment-specific calibration is available. It is nevertheless clear that Grx1-roGFP2 detects nanomolar changes in [GSSG] against a backdrop of millimolar [GSH], in accordance with *in vitro* data and theoretical predictions. For example, the external application of a single H_2O_2 bolus in the low micromolar range (1–10 μM) leads to a reproducible intracellular probe response. Assuming that only a fraction of externally added H_2O_2 enters the cytosol (1) and that cytosolic H_2O_2 is not fully converted into GSSG (given peroxiredoxins and catalase), the sensor response almost certainly corresponds to the detection of nanomolar changes in [GSSG], possibly reaching down to the low nanomolar range.

f. Implications for redox signaling. Interestingly, the dynamic behavior of Grx1-roGFP2 inside living cells may have implications beyond its use as a biosensor. If it is assumed that natural Grx1 target proteins behave similarly to roGFP2, which seems reasonable, they should also be dynamically oxidized (*S*-glutathionylated) and reduced (de-glutathionylated) in response to physiological changes in E_{GSH} (Fig. 15). Grx1-roGFP2 clearly demonstrates that glutathionylation can drive the formation of stable disulfide bonds, suggesting that Grx1 target proteins frequently convert *S*-glutathionylation into intra- or intermolecular disulfide bonds (if a second thiol is available nearby). Naturally, the extent of Grx1-catalyzed

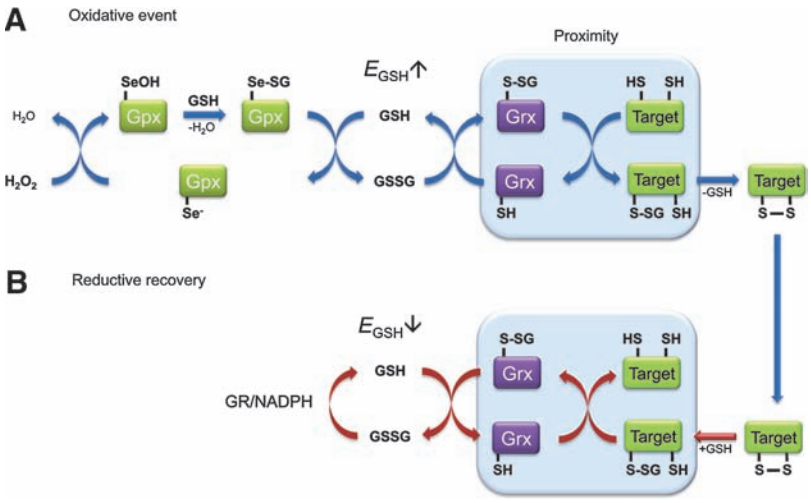

FIG. 15. Glutaredoxin as a general mediator of reversible protein thiol oxidation in H_2O_2 signaling. Grx may play a general role in reversible protein thiol oxidation. (**A**) Through the action of glutathione peroxidases, H_2O_2 transiently increases E_{GSH}. In response, oxidation-sensitive proteins co-localized with Grx become *S*-glutathionylated. Glutathionylation may in turn lead to disulfide bond formation. (**B**) Upon renormalization of E_{GSH}, GSH attacks the same disulfide bonds and Grx catalyzes de-glutathionylation of the same proteins. (For interpretation of the references to color in this figure legend, the reader is referred to the web version of this article at www.liebertonline.com/ars).

disulfide formation would depend on the respective dithiol/disulfide midpoint potential, which is certain to differ among target proteins. Although Grx1 is predominantly known for its reductive functions, protein *S*-glutathionylation is increasingly discussed as a possible pro-oxidative function of Grx1 (82). The dynamic behavior of Grx1-roGFP2 in living cells now clearly demonstrates that Grx1 catalyzes dynamically in both directions and that this happens readily within the physiological range of E_{GSH}. Accordingly, a large set of thiol proteins may be redox-regulated by Grx1-mediated real-time equilibration with the 2GSH/GSSG redox couple. However, Grx1-roGFP2 also demonstrates that co-localization between Grx1 and target protein is very important, and it may be that only those Grx1 target proteins in close proximity to endogenous Grx1 are efficiently coupled to E_{GSH}. ASK1 and Procaspase-3 may be a case in point as these proteins seem to associate directly with Grx1 (96, 112).

Grx-mediated protein oxidation may also help to understand the phenomenon of H_2O_2-based signaling. An important question is how H_2O_2 can oxidize redox-regulated proteins efficiently and specifically, despite competition by highly efficient and abundant scavenger systems. It has been suggested that regulatory protein thiol oxidation by H_2O_2 may sometimes, if not frequently, be an indirect process (130). The Grx1-roGFP2 probe potentially exemplifies such an indirect pathway (Fig. 15) in that H_2O_2 facilitates protein thiol oxidation through the GSSG intermediate. In other words, ultrasensitive H_2O_2-scavenging enzymes (*e.g.*, glutathione peroxidases in mammalian cells or ascorbate peroxidase together with dehydroascorbate reductase in plant cells) may act as highly efficient initiators of oxidative signaling by generating transient bursts of GSSG. The resulting pro-oxidative shift in E_{GSH} then triggers Grx-mediated protein oxidation in those oxidation-sensitive proteins that are in close physical association with appropriate Grxs, but not in others (Fig. 15A). Once E_{GSH} normalizes by the action of GRs, Grx catalyzes the reduction of the same proteins (Fig. 15B). It may be speculated that Grx1-roGFP2 dynamically responds to endogenous H_2O_2 signals precisely because it mimics a natural pathway of regulatory protein thiol oxidation.

B. Coupling roGFPs to thioredoxins

1. The concept behind Trx1-roGFP2. The successful redox coupling of Grx1 and roGFP2 and the considerations regarding the increased local concentration and therefore probability of interaction (see Section III.A.2.a) suggested the possibility that a Trx-roGFP2 fusion protein may likewise serve as reversible probe for the Trx redox state. This possibility is conceivable for two reasons. First, Trx has been observed to become transiently oxidized during oxidative stress and redox signaling (45), thus suggesting that Trx is not kept in the reduced state at all times. Second, disulfide exchange between Trx and substrates is reversible in principle, and prokaryotic Trxs were previously shown to be able to act as oxidases (23, 113). Depending on the position of the equilibrium, Trx may thus oxidize roGFP by dithiol/disulfide exchange. In principle, this may allow visualization of transient Trx oxidation, potentially associated with oxidative signaling events. Assuming that specific and efficient equilibration between Trx1 and roGFP2 occurs in a fusion protein, the following Nernst relationship should apply:

$$E_{Trx1} = E^{\circ\prime}_{Trx1} - \frac{RT}{2F}\ln\left(\frac{1 - OxD_{Trx1}}{OxD_{Trx1}}\right)$$
$$= E^{\circ\prime}_{roGFP2} - \frac{RT}{2F}\ln\left(\frac{1 - OxD_{roGFP2}}{OxD_{roGFP2}}\right) = E_{roGFP2}$$

The midpoint potential of the active site dithiol–disulfide pair of human Trx1 has been determined as −230 mV (128). The midpoint potential of roGFP2 is yet more negative (Fig. 16A), leading to the prediction that only a highly reduced Trx1 would keep roGFP2 in the reduced state. Any weak increase in Trx1 oxidation would translate into substantial roGFP2 oxidation. Specifically, a shift towards 2% Trx1 oxidation should entail 50% roGFP2 oxidation (Fig. 16B).

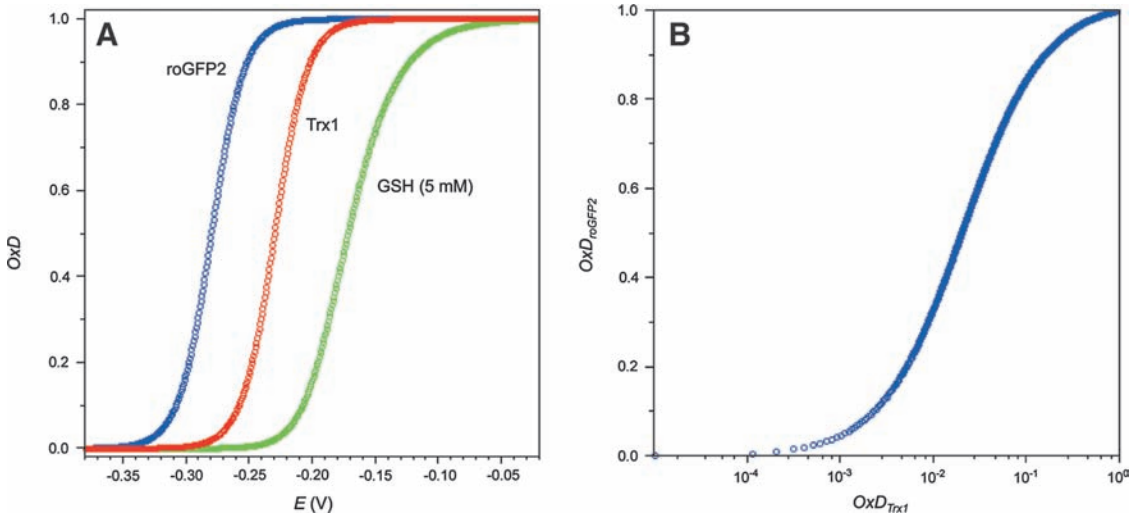

FIG. 16. Theoretical thermodynamic relationship between the roGFP2 and Trx1 redox couples. (**A**) Relationship between *OxD* and *E*, shown for roGFP2 (*blue curve*), Trx1 (*red curve*), and, for comparison, GSH at 5 m*M* (*green curve*). (**B**) Minor increases in Trx1 oxidation are expected to entail major increases in roGFP2 oxidation. (For interpretation of the references to color in this figure legend, the reader is referred to the web version of this article at www.liebertonline.com/ars).

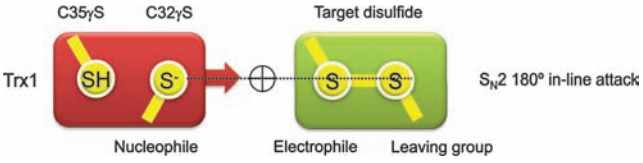

FIG. 17. Bimolecular nucleophilic substitution (S_N2) requires an in-line arrangement between nucleophile, electrophile, and leaving group. The nucleophilic sulfur of Trx (C32γS) needs to be precisely positioned for the 180° in-line attack on the target disulfide (*cross hairs*). The geometry of this mechanism imposes restrictions for enzyme substrate interactions. (For interpretation of the references to color in this figure legend, the reader is referred to the web version of this article at www.liebertonline.com/ars).

2. The geometrical limits of thiol–disulfide exchange. All these theoretical predictions assume effective equilibration by thiol–disulfide exchange. However, it turned out that human Trx1 does not interact with roGFP2. Neither does fully reduced Trx (coupled to the complete Trx system) target oxidized roGFP, nor does the reverse reaction take place (40). Likewise, the same observation applies to rxYFP and Trx (93). Why does roGFP2 readily interact with Grx, but not with Trx? It is not well understood by which criteria Trx1 targets particular disulfide bonds (while ignoring others, even if well exposed). The stereochemical conformation of the roGFP2 disulfide bridge is rather unusual. Bonds of this type are known as 'right-handed staples' or 'cross-stranded' disulfides (55, 105, 132). Interestingly, this atypical geometry is shared by several disulfides known to be readily reduced by Trx [*e.g.*, a disulfide in the CD4 cell surface receptor (73) and another in BASI (barley α-amylase/subtilisin inhibitor)] (69). On these grounds, the disulfide on roGFP2 would appear to be a likely target for Trx. It is well exposed on the barrel surface and the 'staple' geometry is compatible with Trx-mediated reduction in other proteins. The most likely explanation for the resistance of the roGFP2 disulfide bond against Trx is a structural constraint imposed by the reaction mechanism. In general, thiol–disulfide exchange reactions proceed by bimolecular nucleophilic substitution (S_N2). This implies that the three participating sulfur atoms (nucleophile, electrophile, and leaving group) have to be arranged in a straight line (Fig. 17). It is somewhat surprising that the implications of S_N2 geometry for protein disulfide exchange interactions are rarely discussed in the literature, with only few exceptions (28, 52, 129).

The S_N2 constraint likely explains why right-handed 'staple' disulfides are preferentially targeted by Trx in certain other proteins, but not in roGFP2 (or rxYFP). When a 'staple' disulfide bond is positioned on the edge of a β-sheet (as in BASI), the interface encountering the active site surface of Trx is relatively flat. The point in space that needs to be reached by the nucleophilic sulfur of C32 in order to mount an in-line attack is unobstructed by side-chains (Fig. 18). More specifically, it appears to be essential that the two residues flanking the target cysteine do not project their side chains into the direction of Trx. In fact, the β-sheet configuration effectively prevents steric interference of this kind. Any side chain (even alanine) projecting towards Trx would be predicted to get into steric conflict with W31 and P34 on Trx1, two highly conserved residues flanking the nucleophilic C32.

These considerations may also explain why the situation is fundamentally different in the case of the roGFP2-Trx interaction: The roGFP2 disulfide is not located at the edge of the β-sheet and the sulfur–sulfur axis of the roGFP disulfide bond lies flat and parallel to the barrel surface. Therefore, most likely, the nucleophilic sulfur of Trx, located in a narrow groove between W31, P34, and other residues, is sterically prevented from positioning itself for the S_N2 reaction (Figs. 19 and 20A).

The same considerations may also explain why the roGFP2 disulfide bond is a very good substrate for the Grx/GSH system (Fig. 20B). Most likely, the small glutathione molecule can easily reach the position required for in line attack on the roGFP2 disulfide bond. The resulting roGFP2–S-SG mixed disulfide bond is much more accessible, because it is not as close to the barrel surface. In addition, the sulfur-containing bonds of roGFP2–S-SG are rotatable, thus offering many alternative positions for subsequent nucleophilic attack. This may explain why there is no steric problem for Grx to attack roGFP2–S-SG. It may be asked if Trx would also be able to attack and reduce the roGFP2-S-SG conjugate with its more accessible disulfide bond. *In vitro* experiments indicate that this is not the case (Gutscher *et al.*, unpublished data), suggesting that either roGFP–S-SG is still not accessible enough for Trx, or that Trx somehow discriminates against protein–S-SG mixed disulfides as substrates.

In conclusion, it seems unlikely that a working Trx-roGFP redox relay can be created. On the positive side, the fact that Trx refuses to interact with the roGFP2 intramolecular disulfide bond (and also with the roGFP2-S-SG disulfide bond) strengthens the concept that roGFP2 (and especially Grx1-roGFP2) really are highly specific probes for 2GSH/GSSG.

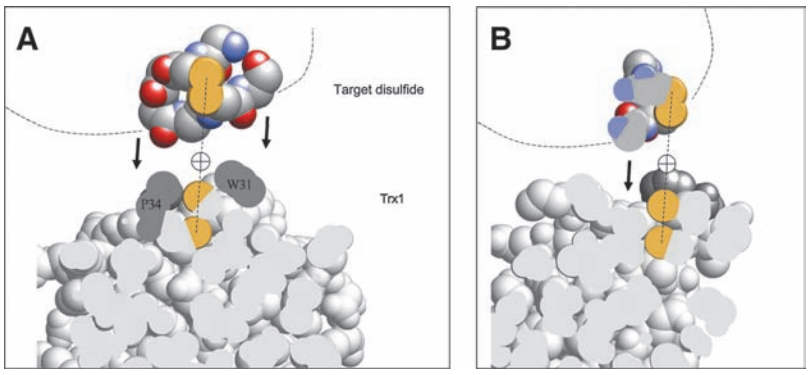

FIG. 18. Molecular model for the encounter between Trx1 and a 'staple' disulfide bond located on a β-sheet edge. The geometry allows the electrophilic sulfur atom to reach the S_N2 attack point (*cross hairs*). The flat edge of the β-sheet allows positioning of the electrophilic sulfur atom between conserved residues W31 and P34 without steric interference by side chains. (**A**) Front view and (**B**) side view rotated by 90°. The figure is based on PDB entries 1ERT (thioredoxin) and 1AVA (staple disulfide bond with surrounding β-sheet). (For interpretation of the references to color in this figure legend, the reader is referred to the web version of this article at www.liebertonline.com/ars).

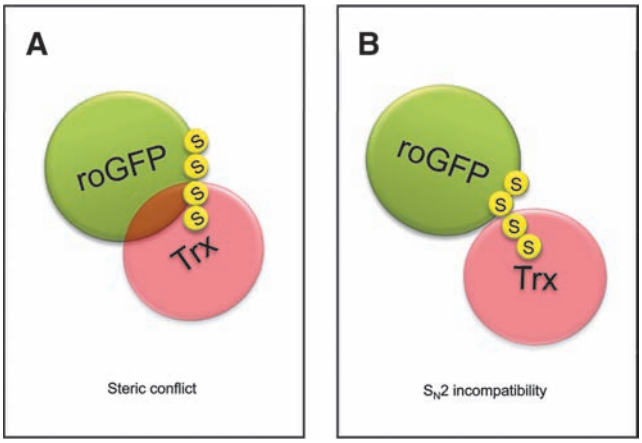

FIG. 19. A likely explanation for the lack of disulfide exchange between roGFP2 and Trx1. Proper in-line alignment for S_N2 is prevented by massive steric conflict (**A**), while the angled approach is not compatible with the geometric necessities of a S_N2 reaction (**B**). (For interpretation of the references to color in this figure legend, the reader is referred to the web version of this article at www.liebertonline.com/ars).

Of course, it remains possible that certain Trxs from other organisms or organelles, possibly those with a shallower active site groove (*i.e.*, with a more exposed nucleophile), can engage in thiol–disulfide exchange with roGFPs. However, even if a disulfide-exchanging Trx/roGFP combination can be found, the usefulness of the corresponding fusion protein to visualize the native endogenous Trx redox state would be quite uncertain. The bulky roGFP domain may sterically hinder the interaction of Trx with its native redox partners TrxR and the peroxiredoxins. In that case the probe may not properly reflect the native redox state of Trx. Moreover, the interpretation of the probe response may be further complicated as slow interactions with the endogenous GSH/Grx system may take place in parallel. It seems that fresh ideas are needed to finally develop a genetically encoded redox probe specific to the Trx redox state (see also Section V.A.2).

C. Coupling roGFPs to peroxidases

1. The concept behind roGFP2-Orp1. Is it possible to convert roGFPs into specific probes for H_2O_2 or other peroxides? Peroxiredoxins and glutathione peroxidases are highly efficient and selective H_2O_2 receptors. Intriguingly, some peroxidases have been found to transmit oxidation to other proteins. The best studied example is the regulatory oxidation of the transcription factor Yap1 by the peroxidase Orp1 (Gpx3) in yeast (24). This finding led to the question if Orp1 would accept roGFP in place of its natural target protein, Yap1. To test the idea, roGFP2 was fused to Orp1 to create a redox relay in which roGFP2 replaces Yap1 and the linker enforces proximity (41) (Fig. 21). In fact, Orp1 was found to form a highly efficient redox relay with roGFP2. *In vitro*, Orp1 mediated near-stoichiometric oxidation of roGFP2 by H_2O_2, converting almost every H_2O_2 molecule into a roGFP2 disulfide bridge. Moreover, the Orp1-roGFP2 redox couple effectively converts physiological H_2O_2 signals into measurable fluorescent signals in living cells (41).

The intracellular mechanism of the roGFP2-Orp1 redox relay was found to be based on dithiol-disulfide exchange between the two domains (Fig. 22). Oxidation of Orp1 by H_2O_2 first generates an intramolecular disulfide bond between C36 and C82. In a second step, the disulfide bond is transferred to roGFP2 by thiol–disulfide exchange (41). The Orp1 C36/C82 dithiol/disulfide midpoint potential was measured as -255 (± 8) mV at pH 6.0 (72), suggesting a value of -314 mV at pH 7.0 by extrapolation (based on the -59 mV per pH unit dependence). Considering thiol–disulfide exchange between Orp1 and roGFP2, Orp1 should be rather inefficient in oxidizing roGFP2 (50% sensor oxidation would require approx. 90% Orp1 oxidation). However, in situations where Orp1 encounters H_2O_2 frequently, it will be kept at 100% oxidation by H_2O_2 and thus transfer oxidative equivalents to roGFP2 very efficiently. Thus, Orp1 can be seen as a redox catalyst mediating electron flow between the H_2O_2/H_2O pair (approx. $+1350$ mV at pH 7) and the $roGFP2_{ox}/roGFP2_{red}$ redox pair.

The roGFP2-Orp1 relay demonstrates dynamic behavior in living cells. Thus, it is important to ask how the probe is reduced inside cells. In principle, there are two possibilities. Similar to conventional roGFP2, the roGFP2 disulfide within the fusion protein may be reduced by GSH. This would depend on endogenous Grx and be rather slow. Based on the thermodynamic relationship between roGFP2 and Orp1, it appears more likely that roGFP2 passes the disulfide bond back to Orp1. This leads to the question of how Orp1 is reduced inside living cells. In yeast, Trx is the natural reductant

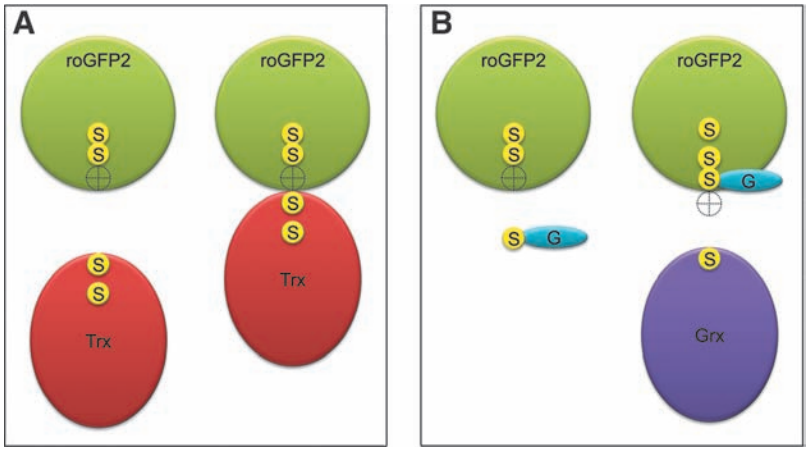

FIG. 20. Differing sterical constraints for Trx and Grx. Most likely, thioredoxin ignores roGFP2 because its nucleophilic cysteine cannot take the S_N2 attack position (*cross hairs*) (**A**). In contrast, glutathione is small enough to position itself and engage in disulfide exchange with roGFP2. The disulfide bridge of the resulting glutathione–roGFP2 conjugate is more accessible and thus engages successfully with Grx (**B**). (For interpretation of the references to color in this figure legend, the reader is referred to the web version of this article at www.liebertonline.com/ars).

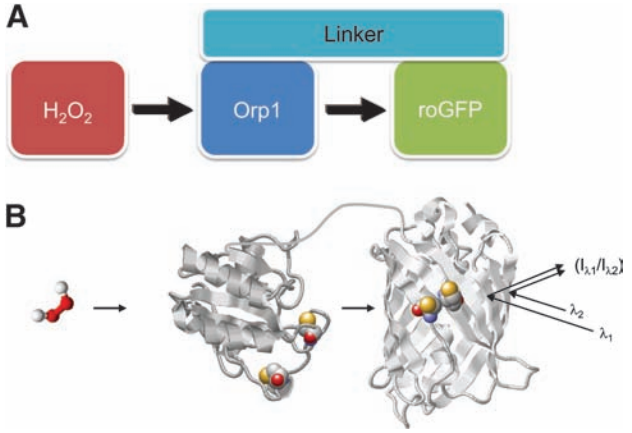

FIG. 21. Principle of the roGFP2–Orp1 redox relay. (**A**) RoGFP2-linked Orp1 efficiently catalyzes equilibration between H_2O_2 and roGFP2. (**B**) Structural model showing H_2O_2 and the roGFP2-Orp1 fusion protein in the reduced state. The redox state of roGFP2 is obtained by ratiometric fluorescence intensity (I) measurements at two different excitation wavelengths (λ_1, λ_2). (For interpretation of the references to color in this figure legend, the reader is referred to the web version of this article at www.liebertonline.com/ars).

of Orp1 and this may also be the case in mammalian cells. The −314 mV midpoint potential of Orp1 is compatible with its reduction by human Trx1 ($E^{\circ\prime}_{Trx1} = -230$ mV), if the Trx1 pool is highly reduced ($OxD_{Trx} < 1\%$). At present, it is not known if roGFP2–Orp1 is exclusively reduced by Trx1, or, potentially, by both Trx1 and GSH/Grx1. In any case, as roGFP2–Orp1 reports on the thiol redox state of Orp1, its response is best seen as a reflection of the balance between H_2O_2-mediated thiol oxidation and (Trx- and/or Grx-mediated) thiol reduction.

2. Implications for H_2O_2 signaling. Similar to the potential role of Grx1 in regulatory protein oxidation (Section III.A.2.f.), the fact that roGFP2-Orp1 converts physiological concentrations of H_2O_2 into protein disulfide bonds may as well have implications beyond its use as a biosensor, namely for the mechanism of H_2O_2 signaling. Apparently, Orp1 is not mechanistically restricted to use Yap1 as the recipient of oxidative equivalents and thus harbors a more general ability to act as a thiol oxidase for other proteins (41). In turn, this may suggest that certain other peroxidases, peroxiredoxins, and/or members of the glutathione peroxidase family have a similar intrinsic capacity to promote the oxidation of other proteins. In fact, the human selenocysteine-based glutathione peroxidase Gpx4 was already implicated in the disulfide cross-linking of protamines and is also capable of mediating the oxidation of roGFP2 in living cells (41). Close prepositioning between peroxidases and target proteins likely is critical for the transfer of oxidizing equivalents. Only protein thiols close to the peroxidase active site are likely to intercept the peroxidatic cycle. If roGFP2-Orp1 is indicative of a more general principle of H_2O_2 signaling, a major task for the future is to identify and study natural peroxidase-target relationships in higher eukaryotic cells.

IV. Other Genetically Encoded Redox Probes

All genetically encoded redox probes discussed so far are based on redox-sensitive FPs. However, redox probes can also be developed from non-redox-sensitive FPs. In principle, any conformational change associated with protein redox state may be exploited to change the fluorescent properties of a FP which is not redox-active by itself. One possible approach is the insertion of cpYFP into a redox-active protein domain, in a way comparable to previously established non-redox probes (*e.g.*, Pericam Ca^{2+} sensors) where a conformational change couples the process of interest to a change in fluorescence. Only a single redox probe (HyPer) falling into this category has been reported so far (Section IV.A). Another approach to convert a redox-dependent conformational change into a fluorescent signal is fluorescence resonance energy transfer (FRET) (Section IV.B).

A. HyPer: A cpYFP-based redox probe

1. The concept behind HyPer. HyPer has been designed to serve as a specific indicator for intracellular H_2O_2 (6). It is built on the H_2O_2-sensing regulatory domain (RD) of the prokaryotic transcription factor OxyR. The active site cysteine of OxyR-RD (C199) readily reacts with H_2O_2 to form a cysteine sulfenic acid (S-OH) which subsequently condenses with a second cysteine in the same domain (C208) to form an intramolecular disulfide bridge. In the reduced state, C199 and C208 are separated by 17 Å and a substantial conformational change, predominantly affecting peptide segment 205-222, takes place upon oxidation (20). To create HyPer, Belousov and colleagues inserted cpYFP between residues 205 and 206 of OxyR-RD. The cpYFP moiety was further optimized for folding and chromophore maturation, and the Y203F mutation was introduced to visualize the protonated form of the cpYFP chromophore. The resulting cpYFP–OxyR-RD chimera, named HyPer, displays a single emission maximum at 516 nm and two excitation maxima at 420 (protonated chromophore) and 500 nm (deprotonated chromophore).

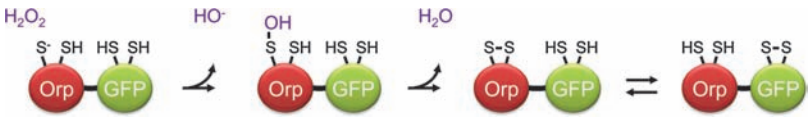

FIG. 22. Molecular mechanism of the roGFP2–Orp1 biosensor. Upon encountering H_2O_2, the Orp1 domain forms a sulfenic acid residue which is rapidly converted into a disulfide bridge within the same domain. Subsequent thiol–disulfide exchange between the Orp1 and roGFP2 domains leads to formation of the roGFP2 disulfide bridge. (For interpretation of the references to color in this figure legend, the reader is referred to the web version of this article at www.liebertonline.com/ars).

Importantly, the conformational influence of disulfide bond formation leads to a ratiometric shift with the 420 nm peak decreasing and the 500 nm peak increasing. HyPer was shown to detect nanomolar H_2O_2 *in vitro* and, when expressed in cells, to respond to micromolar H_2O_2 added externally. HyPer also allowed detection of oxidative changes induced by growth factors (6, 70). The maximal ratiometric dynamic range *in vitro* was reported as 3- to 4-fold. However, ratiometric changes in live cell imaging after physiological stimuli were more moderate (*i.e.*, a 15% ratio increase after NGF stimulation), indicating that accurate measurements of physiologically relevant events can be technically demanding.

2. How specific is HyPer as a probe for H_2O_2? How accurately does the HyPer signal reflect dynamic variations in endogenous H_2O_2 levels? On the one hand, there is little doubt that the OxyR regulatory domain is highly selective in its reactivity towards H_2O_2. On the other hand, the cpYFP moiety of HyPer does not sense H_2O_2 directly. Instead, the fluorescence response reflects the thiol redox state of OxyR-RD. The thiol redox state of OxyR-RD is the result of the dynamic interplay between disulfide formation and disulfide reduction. This leads to the question of how the HyPer disulfide bond is reduced within eukaryotic cells. In *E. coli* the disulfide form of OxyR is reduced by the glutathione system, specifically by GSH under catalysis of Grx1 (136). It is likely that reduction of HyPer in eukaryotic cells also depends on the glutathione system. Therefore, in principle, events curtailing the disulfide reducing function of the glutathione system (*e.g.*, limiting NADPH levels or loss of GSH) may well shift the balance towards increased HyPer oxidation, even if H_2O_2 levels remain the same.

Regarding the role of the glutathione system, there is an additional concern: If Grx mediates reduction of the HyPer disulfide it may also catalyze the reverse reaction, namely disulfide formation, based on the Nernst relationship between the glutathione redox couple and the dithiol/disulfide couple of HyPer. Of note, *in vitro*, when purified OxyR is incubated with a combination of GSSG and Grx1 (rather than GSSG alone), it is, on a molar basis, as efficiently oxidized as with H_2O_2 (136). Is it conceivable that Grx-catalyzed oxidation of HyPer by GSSG occurs in intact cells? It is unlikely to be a major concern, at least for the cytosolic compartment. First, oxidation of OxyR-RD by GSSG becomes thermodynamically favorable only at relatively high GSSG concentrations. The midpoint potential of the OxyR dithiol/disulfide couple has been reported as -185 mV (136). Thus, to oxidize HyPer (OxyR) by 10%, an E_{GSH} of -214 mV is required (at $GSH_{total} = 5$ mM this would correspond to $[GSSG] = 165\ \mu M$). As discussed before, measurements with rxYFP, roGFPs, and Grx1-roGFP2 strongly indicate that such a high E_{GSH} is unlikely to occur in the cytosol of living cells under physiological conditions. Second, it is not clear if intracellular Grx levels would be sufficient to support equilibration. Most likely, GSSG-mediated oxidation of HyPer is limited by the local availability of Grx and therefore a slow process. It appears safe to assume that under most circumstances H_2O_2 is the predominant oxidant for HyPer. It should be noted, however, that the midpoint potential of the 2GSH/GSSG redox couple depends on GSH_{total}. The lower the concentration of the total GSH pool, the more favored is HyPer (OxyR) oxidation by GSSG.

With regard to reversibility, HyPer differs fundamentally from Grx1-roGFP2. Grx1-roGFP2 measures the redox potential of a single redox pair by equilibrating with the same. In contrast, HyPer (*i.e.*, OxyR-RD) communicates with two redox pairs simultaneously: $2H_2O/H_2O_2$ and 2GSH/GSSG, thus displaying a fundamental asymmetry between the oxidation and reduction reactions. Obviously, roGFP2-Orp1 is subject to the same mechanistic asymmetry as HyPer. Thus, it is probably more appropriate to consider HyPer a probe for the balance between H_2O_2-mediated disulfide formation and glutathione-mediated disulfide reduction and, correspondingly, roGFP2-Orp1 a probe for the balance between H_2O_2-mediated disulfide formation and (probably Trx-mediated) disulfide reduction. This kind of probe behavior should not be considered a shortcoming, as measuring the thiol oxidation-reduction balance is highly relevant for the investigation of cellular redox signaling.

Finally, another concern that deserves attention is the influence of pH on HyPer fluorescence. From the pH titration curve (6) it appears that the 500/420 excitation ratio is significantly shifted by pH and that a shift of 0.2 pH units can be sufficient to change the ratio as much as full reduction or oxidation. Thus, for practical purposes it seems important to monitor pH changes in the same experiment.

3. Applications of HyPer. HyPer measurements have been successfully applied to study the wound response of zebra fish larvae (90). Cytoplasmic sensor expression was achieved in whole animals by injecting HyPer mRNA into embryos. Local injury of the tail fin produced a localized, graded, and transient HyPer signal. The interpretation of the observed HyPer response as a H_2O_2 signal was supported by the fact that pH changes could not be detected. A fluorogenic dye also indicated oxidant formation under the same conditions, and the signal was dependent on the expression of the NADPH oxidase Duox. Thus, it appears very likely that the observed HyPer response was directly caused by H_2O_2.

B. FRET-based redox probes

Similar to other FRET-based probes (36), conformational changes associated with protein redox states can be exploited to influence the distance between a FRET donor-acceptor pair. Only very few publications investigated the direction of genetically encoded FRET-based redox probes. In general, the FRET strategy requires a redox-active peptide or protein domain. A rather simple concept is to use a peptide linker harboring two cysteines to form an intramolecular disulfide bond under oxidative conditions. In a recent study (61), artificial peptide linkers containing cysteine pairs were placed between a FRET pair of enhanced cyan and yellow fluorescent proteins. However, the maximal changes in FRET efficiency were modest and the detection of physiological redox changes remains to be demonstrated. Kinetics and sensitivity may be limiting factors for the peptide linker approach. It is also not clear which cellular redox couples or enzymes would actually interact with peptide linker cysteines, raising questions about specificity. At the present stage, FRET redox probes with short peptide linkers lag behind the other strategies described before. A more sophisticated FRET redox sensor is HSP-FRET (100) in which the redox-sensitive domain of bacterial hsp33 is placed between ECFP and YFP. Expressed in cardiomyocytes,

HSP-FRET detected oxidative changes associated with hypoxia. Future FRET approaches based on protein domains with defined redox behavior and specificity are likely to contribute to the field.

V. Future Directions and Challenges

A. Further development of redox biosensor methodology

The future understanding of interlinked processes in the context of whole organisms will depend on our ability to acquire quantitative data with high resolution in time and space. Generally, quantitative live cell imaging with genetically encoded probes has the potential of fulfilling these demands, albeit only for one or a few physiological parameters at a time. While current redox-sensitive FPs have already shown their potential to deliver quantitative and dynamic information, there is still much room for further improvements and extensions. We here address different options for further tuning of current sensors and for the development of novel probes with altered properties and specificities.

1. Improvements and new modalities

a. Redox probes with different colors. Current ratiometric redox probes based on roGFPs all emit green light of the same wavelength. Thus, comparison of steady state E_{GSH} in different compartments and investigation of interorganellar redox communication often requires separate measurements for each compartment. Simultaneous measurements in two or more subcellular compartments would be more convenient with differentially colored redox probes. A first step in this direction may be the use of rxYFP in combination with roGFPs. It should be possible to employ rxYFP as a *bona fide* ratiometric probe by fusing it to a redox-invariant FP. Previously, the Cl^--sensitivity of YFP has been exploited to generate the Cl^- sensor Clomeleon in which the Cl^--sensitive YFP is fused to the Cl^--insensitive CFP (62). Similarly, translational fusion of rxYFP with an appropriate redox-independent reference fluorophore such as red fluorescent protein (RFP) or even further red-shifted FP variants may be one possibility to enable ratiometric measurements with rxYFP. Obviously, the dynamic range of such a ratiometric probe would be limited by the maximum redox-dependent change in fluorescence of rxYFP and thus not exceed the value of 2.2. Despite considerable overlap between roGFP and rxYFP fluorescence, spectral deconvolution methods allow a clear separation of the two signals. More convenient, however, would be the development of a ratiometric redox-sensitive FPs with emission peaks shifted far more towards the red end of the visible spectrum to avoid interference with roGFP fluorescence.

Following the initial discovery of GFP (111) and dsRed (74), more than 150 distinct fluorescent or colored proteins have been identified from a whole array of different species. Together with the large number of spectral varieties of GFP generated through mutagenesis (135), it can be envisaged that combinatorial approaches may allow for virtually infinite possibilities for further modifications of the current probes. The problem, however, is that it is still extremely difficult to rationally predict sensor properties and design a probe accordingly. In fact, engineering of redox-sensitive disulfides into YFP and GFP are two of only very few examples of rational probe design.

b. Redox probes enabling higher temporal resolution. Grx1-roGFP2 is already highly responsive to changes in E_{GSH} and equilibrates on a second-to-minute time scale. Nevertheless, it may be possible to further shorten the response time of chimeric roGFP-based probes, potentially allowing the detection of highly transient deflections on even shorter time scales. Further kinetic improvements of roGFP-based probes can be envisaged through a combination of approaches previously used to establish second and third generation redox probes (Fig. 4). It is likely that oxidation of roGFP2 within a fusion protein is kinetically limited by the high pK_a (>9) of its cysteines. Thus, the engineering of chimeric roGFP2 to increase cysteine reactivity may result in even faster probes. The pK_a of thiols can be tuned by amino acid residues in close proximity (38). Substitution of residues close to one or both cysteines by arginine or lysine was already shown to increase the reactivity of nonchimeric rxYFP (47) and roGFP1 (13). In addition, it is also conceivable to tune the catalytic properties of the redox enzyme employed within chimeric fusion proteins. For example, a single cysteine variant of yeast Grx1p (with a CPYS active site motif) was more efficient in catalyzing the oxidation of rxYFP than Grx1p with the native CPYC motif (7). Also, a side-by-side comparison of Grx enzymes may identify paralogues or orthologues capable of catalyzing the oxidation and reduction of roGFPs even more efficiently. Finally, the catalytic efficiency of fusion proteins like Grx1-roGFP2 and roGFP2-Orp1 may also be affected by the length of the linker between the two protein domains. The influence of linker length on redox relay efficiency has not been systematically investigated. Obviously, a linker too short would prevent productive inter-domain interactions. On the other side, a very long linker would effectively lower the local Grx concentration experienced by roGFP and thus may also diminish the frequency of productive collisions. As the C-terminus of roGFP emerges from the protein on the same face as the catalytic cysteines, it is likely that the positioning of roGFP2 at the N-terminus of a chimeric construct allows for more flexible interactions between the two domains. Correspondingly, it may be predicted that a linker on the C-terminus of roGFP/rxYFP can be shorter than one at the N-terminus. In fact, rxYFP-Grx1p was created with a linker of just eight amino acids (7), which may approximate the shortest possible linker to allow productive domain interactions.

c. Redox probes with different midpoint potentials. The creation of probes with modified midpoint potential and measuring range is another important topic. roGFPs have been targeted to the ER lumen in human (2, 106), plant (81), and yeast cells (79). In all species, the OxD_{roGFP} in this compartment was found to be beyond the useful dynamic range of the probe (*i.e.,* the redox potential of roGFP2 in the ER was higher than -240 mV). A range of novel roGFP versions with redox potentials of up to -229 mV have been generated (67), but it remains to be seen if these midpoint potentials are sufficiently high to dynamically resolve the actual E_{GSH} in the ER lumen. Although it is possible that roGFPs in the ER reliably equilibrate with 2GSH/GSSG, it cannot be excluded at this stage that roGFPs also interact with Ero1 and members of the PDI family that catalyze the

formation of protein disulfide bonds in the ER (15,109). To ensure preferential equilibration of roGFP with 2GSH/GSSG, it may thus be advisable to use Grx fusion proteins for the ER as well.

d. Redox probes with improved targeting properties. RoGFPs can be specifically targeted to mitochondria in HeLa (40, 49) and plant cells (87, 107) by using appropriate N-terminal targeting sequences. Similarly, Grx1–roGFP2 was successfully targeted to mitochondria in HeLa cells (40). Surprisingly, however, the same Grx1–roGFP2 fusion protein was not imported into mitochondria of *Drosophila* and different plant species despite the use of established species-specific mitochondrial targeting sequences (own unpublished observations). These problems indicated that human Grx1 may prevent correct mitochondrial targeting of the chimeric probe when expressed in heterologous systems. This restriction may be overcome in two different ways, either by using species-specific Grxs for the fusion protein, or alternatively, by inverting the order of domains and fusing Grx1 C-terminally of roGFP2. Indeed, recent results demonstrate that an inverted probe with human Grx1 fused to the C-terminus of roGFP2 (roGFP2-Grx1) with the 30 aa spacer $(GGSGG)_6$ is successfully targeted to mitochondria in transgenic plants (Bausewein and Meyer, unpublished data) and flies (Albrecht and Dick, unpublished data).

2. Novel probes for key redox couples. Redox-sensitive FPs provide a probe scaffold that is amenable to improvement, reconstruction, and expansion. Numerous opportunities for the creation of novel probes can be envisaged. In the following paragraphs we give just a few examples for the possible deployment of redox-sensitive FPs in the design of novel probes.

First of all, peroxidase-roGFP redox relays clearly offer opportunities for further probe development. The finding that the thiol-based peroxidase Orp1 efficiently mediates electron flow between H_2O_2 and roGFP2 (41) suggests that the same principle may also be applicable to other peroxidases. In fact, the selenocysteine-based glutathione peroxidase Gpx4 (also known as phospholipid hydroperoxidase, PHGPx) also mediates roGFP oxidation in a live cell context (41). It is now conceivable that a number of roGFP-peroxidase probes can be created to visualize the intracellular oxidative response of individual peroxidases. In this regard, a potentially attractive goal may be the design of a genetically encoded probe for lipid peroxidation.

Another important goal for the future is the development of the hitherto unavailable Trx-specific redox biosensor. As discussed before, existing roGFPs and rxYFP do not interact with Trxs (see Section III.B). Thus, a different strategy is needed to generate a Trx-sensitive probe. It may be possible to introduce novel disulfide switches into GFP, designed from the outset to be accessible to the Trx active site. It may also be possible to create a chimeric redox relay between a Trx target protein and a roGFP. Yet another possibility may be to insert a Trx-sensitive protein domain directly into the barrel of a redox-insensitive FP. A precedent for the latter strategy is the Ca^{2+}-sensor Camgaroo, in which Ca^{2+}-binding calmodulin was inserted into YFP at position 145 (3, 39).

A probe for the redox pair AA/DHA is also high on the wish list. After disproportionation of two molecules monodehydroascorbate (MDHA) to AA and DHA the reduction of DHA to AA is catalyzed by dehydroascorbate reductase (DHAR) and leads to a mixed glutathione-enzyme disulfide (26, 110). Normally this mixed disulfide would be reduced by GSH to form GSSG, but in analogy to the catalytic mechanism of Grx1–roGFP2 it may also be transferable to roGFP2 where it may trigger disulfide formation and a corresponding change in fluorescence. It remains to be seen if a specific probe for AA/DHA can be build upon these or similar principles.

Another highly desired probe is one for the real-time observation of $NO^{\bullet}$. $NO^{\bullet}$ can undergo nitrosylation reactions with protein and low molecular weight thiols. It is conceivable that a *trans*-nitrosylation reaction targeted to roGFP could trigger formation of the roGFP disulfide bridge. A fusion between roGFP and a primary $NO^{\bullet}$ acceptor protein may thus allow $NO^{\bullet}$ imaging. Recently, proteomic profiling of *S*-nitrosylation identified proteins with unexpected stability of the nitrosothiol group (95). The authors suggest that stable *S*-nitrosylation reflects a protein conformational change that shields the nitrosothiol group. Whether such $NO^{\bullet}$-dependent conformational changes can be exploited for the generation of future $NO^{\bullet}$ probes remains to be tested.

3. Redox biosensor transgenic model organisms. Arguably, one of the ultimate methodological goals of redox biology is the ability to study clearly defined redox processes as they occur in the intact physiological context of the living organism. Genetically encoded redox probes now offer an opportunity to make progress into this direction. Much initial work on the characterization and application of roGFP-based probes has been done in transgenic *Arabidopsis* plants (57, 71, 81, 107). For the near future, it can be expected that the yeast *S. cerevisiae* will also play a major role in this context. Although rxYFP has been initially characterized in yeast (92, 93), the ratiometric behavior of roGFP provides a principle advantage over nonratiometric rxYFP and future work in yeast will likely build on roGFP variants. For example, yeast cells expressing roGFP-based probes may be genetically screened for deviations from steady state redox state and thus help identifying novel regulators of redox homeostasis. Similarly, a variety of genetically tractable model organisms expressing roGFP-based probes or HyPer are currently being created and studied to address diverse biological questions. To our knowledge, the list of transgenic species currently generated in various laboratories includes mice, zebra fish, *C. elegans*, *D. melanogaster*, barley, tobacco, trypanosomes, *Chlamydomonas rheinhardtii,* and *Synechocystis*. It remains to be seen what can be achieved with these transgenic models. In this regard, the expression and application of HyPer in zebra fish larvae is a promising first step (90). To unlock the potential of redox imaging in non-transparent organisms, various technical challenges need to be overcome. For example, the potential use of roGFP-based probes in two-photon imaging will have to be investigated. Another potential direction of technical investigation is the *in situ* chemical conservation of the biosensor redox state and its analysis in tissue sections. An attractive long-term perspective for redox biosensor transgenic mouse models is the comparison between healthy and diseased states and the testing of drugs for their actual *in vivo* influence on defined redox states in defined target tissues.

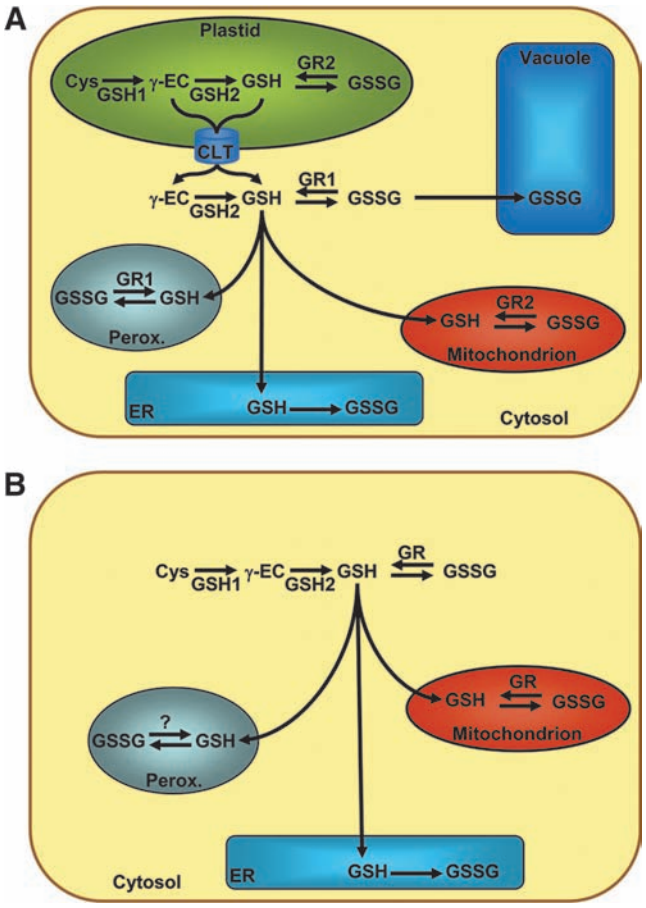

FIG. 23. Biosynthesis and distribution of GSH within eukaryotic cells. (**A**) Subcellular distribution of GSH in *Arabidopsis thaliana*. (**B**) GSH compartmentation in mammalian cells. (For interpretation of the references to color in this figure legend, the reader is referred to the web version of this article at www.liebertonline.com/ars).

B. Applications

Independent of future probe developments, many questions in basic research can be addressed with currently available redox-sensitive FPs. Given the selective equilibration of Grx1–roGFP2 with 2GSH/GSSG, this is especially true with regard to the investigation of glutathione homeostasis and glutathione-dependent transmission of redox signals (80). In addition to applications described in Sections II.B.6 and III.A.2.e, we here exemplarily highlight another application of redox-sensitive FPs, namely to dissect cellular glutathione compartmentalization and interorganellar transport (Section V.B.1). We will then briefly address future probe applications in high throughput screening (Section V.B.2).

1. Exemplary applications in cell biology: Glutathione compartmentalization and transport. Glutathione is required in most subcellular compartments of eukaryotic cells. Despite the ubiquitous need for GSH, its biosynthesis is restricted to either the cytosol in mammalian cells or the plastids and the cytosol in plant cells, which highlights the need for membrane transport of GSH into other organelles (Fig. 23). In *Arabidopsis*, the rate-limiting enzyme GSH1 is exclusively targeted to the plastids while the second enzyme, glutathione synthase (GSH2), is targeted to both plastids and cytosol. This subcellular distribution of the two GSH biosynthetic enzymes implies the need for export of γ-glutamylcysteine (γ-EC) from plastids to supply cytosolic GSH2 with its substrate (97, 123) (Fig. 23A). First candidate proteins for mediating this transport of γ-EC and/or GSH from plastids to the cytosol were identified recently in *Arabidopsis*. Based on high sequence homology to the chloroquine-resistance transporter from *Plasmodium falciparum*, *Pf*CRT, these proteins were named CRT-like transporters (CLTs) (75) (Fig. 23A). Lack of all three CLT isoforms, CLT1, CLT2, and CLT3, caused a slight decrease in total GSH content in shoot tissue, but a more pronounced effect in subcellular compartmentation of GSH was resolved with roGFP2 *in situ*. While plastid-targeted roGFP2 in both wild-type and the triple knockout mutant was almost fully reduced, roGFP2 expressed in the cytosol showed a distinct oxidation in the triple mutant. In contrast to a cytosolic E_{GSH} of about −315 mV in wild-type plants, the cytosolic E_{GSH} in the triple mutant was about 20 mV less reducing. This result is similar to the change in E_{GSH} observed for the partially GSH-deficient *cad2* mutant (Fig. 5). In general, targeting of roGFP to organelles like mitochondria and peroxisomes may provide an excellent opportunity to test candidate proteins for their ability to transport GSH *in situ* and to better understand the dynamics of glutathione compartmentation within eukaryotic cells.

2. High throughput screening. Biosensors on the basis of fluorescent proteins have a huge potential for high throughput screening (HTS) to identify novel drugs affecting specific physiological processes. The use of genetically encoded probes avoids dye loading and washing steps and leads to more robust assays. An example of successful HTS based on GFP-derived sensors is the use of the Cl^--sensitive YFP-H148Q to screen for new classes of potent CFTR activators of the cystic fibrosis transmembrane conductance regulator (CFTR) (68). Rapid quantitative screening of a 60,000 compound library on cells grown on 96-well plates led to the identification of a large number of strong and weak activators. Recently, similar HTS to identify proteins that correct the F508del-CFTR defect was done with YFP–H148Q/I152L (116).

Similar screening approaches can be envisaged with roGFP-based probes to identify novel genes involved in cellular redox homeostasis and drugs affecting defined redox processes. Provided that roGFP variants with appropriate midpoint potentials are available, such screens can be conducted for both reductive and pro-oxidative processes. Although a ratiometric analysis for roGFP is technically more demanding than a single wavelength screen like the one described for Cl^--sensitive YFP, it seems feasible to do such screens on a plate reader, automated microscopes or by FACS. For identifying fast and transient effects on E_{GSH} in a time frame where correction for protein concentration is less critical, it may also be possible to use only a single wavelength to monitor changes in roGFP2 oxidation (121).

C. Overall perspective: Exciting times ahead

Within only few years after their introduction, redox-sensitive FPs have proven to be extremely useful for providing new insights into cellular redox biology. Genetically encoded

redox probes together with high resolution confocal imaging allow the investigation of redox processes in single cells or even at subcellular level. Thus, the application of these probes provides information that was not accessible by other currently available methodologies. The full potential of roGFP-based probes can now be exploited in targeted approaches testing the function of particular genes in cellular redox homeostasis, and in HTS for novel genes and metabolic regulators of intracellular redox homeostasis. The design of novel redox-sensitive FPs is aimed at detecting and quantifying different ROS and other redox active components with the highest possible resolution in time and space. Vice versa, a better mechanistic understanding of how specificity is achieved and maintained in ROS signaling will certainly inspire novel reporter design strategies.

To be statistically meaningful and comparable between different laboratories, quantitative image analysis requires more rigor in experimental design and methodology than comparable qualitative assessments (35). In this context, the exact understanding of probe behavior and detailed *in vitro* and *in vivo* characterization is essential for producing meaningful and interpretable quantitative data. Further expansion of the repertoire of genetically encoded redox-sensitive FPs bears a huge potential for providing new insight into the dynamic behavior of the cellular redox system with minimal perturbation from outside. With the rapidly increasing number of applications based on genetically encoded redox probes and better mechanistic understanding of thiol-dependent redox processes, exciting times are ahead for the growing field of redox biology.

Acknowledgments

The authors gratefully acknowledge funding of their work from the German Research Foundation (DFG), the European Commission and the Landesstiftung Baden-Württemberg.

References

1. Antunes F and Cadenas E. Estimation of H_2O_2 gradients across biomembranes. *FEBS Lett* 475: 121–126, 2000.
2. Austin CD, Wen X, Gazzard L, Nelson C, Scheller RH, and Scales SJ. Oxidizing potential of endosomes and lysosomes limits intracellular cleavage of disulfide-based antibody-drug conjugates. *Proc Natl Acad Sci USA* 102: 17987–17992, 2005.
3. Baird GS, Zacharias DA, and Tsien RY. Circular permutation and receptor insertion within green fluorescent proteins. *Proc Natl Acad Sci USA* 96: 11241–11246, 1999.
4. Barhoumi R, Bailey RH, and Burghardt RC. Kinetic analysis of glutathione in anchored cells with monochlorobimane. *Cytometry* 19: 226–234, 1995.
5. Becker T, Hritz J, Vogel M, Caliebe A, Bukau B, Soll J, and Schleiff E. Toc12, a novel subunit of the intermembrane space preprotein translocon of chloroplasts. *Mol Biol Cell* 15: 5130–5144, 2004.
6. Belousov VV, Fradkov AF, Lukyanov KA, Staroverov DB, Shakhbazov KS, Terskikh AV, and Lukyanov S. Genetically encoded fluorescent indicator for intracellular hydrogen peroxide. *Nat Methods* 3: 281–286, 2006.
7. Björnberg O, Ostergaard H, and Winther JR. Mechanistic insight provided by glutaredoxin within a fusion to redox-sensitive yellow fluorescent protein. *Biochemistry* 45: 2362–2371, 2006.
8. Brach T, Soyk S, Müller C, Hinz G, Hell R, Brandizzi F, and Meyer AJ. Noninvasive topology analysis of membrane proteins in the secretory pathway. *Plant J* 57: 534–541, 2009.
9. Brejc K, Sixma TK, Kitts PA, Kain SR, Tsien RY, Ormo M, and Remington SJ. Structural basis for dual excitation and photoisomerization of the *Aequorea victoria* green fluorescent protein. *Proc Natl Acad Sci USA* 94: 2306–2311, 1997.
10. Buchanan BB. Role of light in the regulation of chloroplast enzymes. *Annu Rev Plant Physiol* 31: 341–374, 1980.
11. Cabibbo A, Pagani M, Fabbri M, Rocchi M, Farmery MR, Bulleid NJ, and Sitia R. ERO1-L, a human protein that favors disulfide bond formation in the endoplasmic reticulum. *J Biol Chem* 275: 4827–4833, 2000.
12. Cairns NG, Pasternak M, Wachter A, Cobbett CS, and Meyer AJ. Maturation of Arabidopsis seeds is dependent on glutathione biosynthesis within the embryo. *Plant Physiol* 141: 446–455, 2006.
13. Cannon MB and Remington SJ. Re-engineering redox-sensitive green fluorescent protein for improved response rate. *Protein Sci* 15: 45–57, 2006.
14. Cannon MB and Remington SJ. Redox-sensitive green fluorescent protein: Probes for dynamic intracellular redox responses. A review. *Methods Mol Biol* 476: 51–65, 2008.
15. Chakravarthi S, Jessop CE, and Bulleid NJ. The role of glutathione in disulphide bond formation and endoplasmic-reticulum-generated oxidative stress. *EMBO Rep* 7: 271–275, 2006.
16. Chang MCY, Pralle A, Isacoff EY, and Chang CJ. A selective, cell-permeable optical probe for hydrogen peroxide in living cells. *J Am Chem Soc* 126: 15392–15393, 2004.
17. Chattoraj M, King BA, Bublitz GU, and Boxer SG. Ultra-fast excited state dynamics in green fluorescent protein: Multiple states and proton transfer. *Proc Natl Acad Sci USA* 93: 8362–8367, 1996.
18. Chew O, Whelan J, and Millar AH. Molecular definition of the ascorbate-glutathione cycle in *Arabidopsis* mitochondria reveals dual targeting of antioxidant defenses in plants. *J Biol Chem* 278: 46869–46877, 2003.
19. Chi AY, Waypa GB, Mungai PT, and Schumacker PT. Prolonged hypoxia increases ROS signaling and RhoA activation in pulmonary artery smooth muscle and endothelial cells. *Antioxid Redox Signal* 12: 603–610, 2010.
20. Choi H, Kim S, Mukhopadhyay P, Cho S, Woo J, Storz G, and Ryu S. Structural basis of the redox switch in the OxyR transcription factor. *Cell* 105: 103–113, 2001.
21. Cobbett CS, May MJ, Howden R, and Rolls B. The glutathione-deficient, cadmium-sensitive mutant, *cad2-1*, of *Arabidopsis thaliana* is deficient in γ-glutamylcysteine synthetase. *Plant J* 16: 73–78, 1998.
22. D'Autreaux B and Toledano MB. ROS as signalling molecules: Mechanisms that generate specificity in ROS homeostasis. *Nat Rev Mol Cell Biol* 8: 813–824, 2007.
23. Debarbieux L and Beckwith J. On the functional interchangeability, oxidant versus reductant, of members of the thioredoxin superfamily. *J Bacteriol* 182: 723–727, 2000.
24. Delaunay A, Pflieger D, Barrault MB, Vinh J, and Toledano MB. A thiol peroxidase is an H_2O_2 receptor and redox-transducer in gene activation. *Cell* 111: 471–481, 2002.
25. Desireddi JR, Farrow KN, Marks JD, Waypa GB, andSchumacker PT. Hypoxia increases ROS signaling and cytosolic Ca^{2+} in pulmonary artery smooth muscle cells of mouse lungs slices. *Antioxid Redox Signal* 12: 595–602, 2010.

26. Dixon DP, Davis BG, and Edwards R. Functional divergence in the glutathione transferase superfamily in plants. Identification of two classes with putative functions in redox homeostasis in *Arabidopsis thaliana*. *J Biol Chem* 277: 30859–30869, 2002.
27. Dooley CT, Dore TM, Hanson GT, Jackson WC, Remington SJ, and Tsien RY. Imaging dynamic redox changes in mammalian cells with green fluorescent protein indicators. *J Biol Chem* 279: 22284–22293, 2004.
28. Eckers E, Bien M, Stroobant V, Herrmann JM, and Deponte M. Biochemical characterization of dithiol glutaredoxin 8 from *Saccharomyces cerevisiae*: The catalytic redox mechanism redux. *Biochemistry* 48: 1410–1423, 2009.
29. Elofsson A and Heijne G. Membrane protein structure: Prediction versus reality. *Annu Rev Biochem* 76: 125–140, 2007.
30. Elsliger MA, Wachter RM, Hanson GT, Kallio K, and Remington SJ. Structural and spectral response of green fluorescent protein variants to changes in pH. *Biochemistry* 38: 5296–52301, 1999.
31. Eubel H, Meyer EH, Taylor NL, Bussell JD, O'Toole N, Heazlewood JL, Castleden I, Small ID, Smith SM, and Millar AH. Novel proteins, putative membrane transporters, and an integrated metabolic network are revealed by quantitative proteomic analysis of *Arabidopsis* cell culture peroxisomes. *Plant Physiol* 148: 1809–1829, 2008.
32. Fernandes AP and Holmgren A. Glutaredoxins: Glutathione-dependent redox enzymes with functions far beyond a simple thioredoxin backup system. *Antioxid Redox Signal* 6: 63–74, 2004.
33. Foreman J, Demidchik V, Bothwell JH, Mylona P, Miedema H, Torres MA, Linstead P, Costa S, Brownlee C, Jones JD, Davies JM, and Dolan L. Reactive oxygen species produced by NADPH oxidase regulate plant cell growth. *Nature* 422: 442–446, 2003.
34. Frand AR and Kaiser CA. Ero1p oxidizes protein disulfide isomerase in a pathway for disulfide bond formation in the endoplasmic reticulum. *Mol Cell* 4: 469–477, 1999.
35. Fricker M, Runions J, and Moore I. Quantitative fluorescence microscopy: From art to science. *Annu Rev Plant Biol* 57: 79–107, 2006.
36. Frommer WB, Davidson MW, and Campbell RE. Genetically encoded biosensors based on engineered fluorescent proteins. *Chem Soc Rev* 38: 2833–2841, 2009.
37. Gallogly MM, Starke DW, and Mieyal JJ. Mechanistic and kinetic details of catalysis of thiol-disulfide exchange by glutaredoxins and potential mechanisms of regulation. *Antioxid Redox Signal* 11: 1059–1081, 2009.
38. Gilbert HF. Molecular and cellular aspects of thiol-disulfide exchange. *Adv Enzymol Relat Areas Mol Biol* 63: 69–172, 1990.
39. Griesbeck O, Baird GS, Campbell RE, Zacharias DA, and Tsien RY. Reducing the environmental sensitivity of yellow fluorescent protein. Mechanism and applications. *J Biol Chem* 276: 29188–29194, 2001.
40. Gutscher M, Pauleau AL, Marty L, Brach T, Wabnitz GH, Samstag Y, Meyer AJ, and Dick TP. Real-time imaging of the intracellular glutathione redox potential. *Nat Methods* 5: 553–559, 2008.
41. Gutscher M, Sobotta MC, Wabnitz GH, Ballikaya S, Meyer AJ, Samstag Y, and Dick TP. Proximity-based protein thiol oxidation by H_2O_2-scavenging peroxidases. *J Biol Chem* 284: 31532–31540, 2009.
42. Guzy RD, Sharma B, Bell E, Chandel NS, and Schumacker PT. Loss of the SdhB, but Not the SdhA, subunit of complex II triggers reactive oxygen species-dependent hypoxia-inducible factor activation and tumorigenesis. *Mol Cell Biol* 28: 718–731, 2008.
43. Haga S, Remington SJ, Morita N, Terui K, and Ozaki M. Hepatic ischemia induced immediate oxidative stress after reperfusion and determined the severity of the reperfusion-induced damage. *Antioxid Redox Signal* 11: 2563–2572, 2009.
44. Hakansson KO and Winther JR. Structure of glutaredoxin Grx1p C30S mutant from yeast. *Acta Crystallogr D Biol Crystallogr* 63: 288–294, 2007.
45. Halvey PJ, Watson WH, Hansen JM, Go YM, Samali A, and Jones DP. Compartmental oxidation of thiol–disulphide redox couples during epidermal growth factor signalling. *Biochem J* 386: 215–219, 2005.
46. Hansen JM, Go YM, and Jones DP. Nuclear and mitochondrial compartmentation of oxidative stress and redox signaling. *Annu Rev Pharmacol Toxicol* 46: 215–234, 2006.
47. Hansen RE, Ostergaard H, and Winther JR. Increasing the reactivity of an artificial dithiol–disulfide pair through modification of the electrostatic milieu. *Biochemistry* 44: 5899–5906, 2005.
48. Hansen RE, Roth D, and Winther JR. Quantifying the global cellular thiol–disulfide status. *Proc Natl Acad Sci USA* 106: 422–427, 2009.
49. Hanson GT, Aggeler R, Oglesbee D, Cannon M, Capaldi RA, Tsien RY, and Remington SJ. Investigating mitochondrial redox potential with redox-sensitive green fluorescent protein indicators. *J Biol Chem* 279: 13044–13053, 2004.
50. Hashemy SI, Johansson C, Berndt C, Lillig CH, and Holmgren A. Oxidation and S-nitrosylation of cysteines in human cytosolic and mitochondrial glutaredoxins: Effects on structure and activity. *J Biol Chem* 282: 14428–14436, 2007.
51. Heazlewood JL, Tonti–Filippini JS, Gout AM, Day DA, Whelan J, and Millar AH. Experimental analysis of the *Arabidopsis* mitochondrial proteome highlights signaling and regulatory components, provides assessment of targeting prediction programs, and indicates plant-specific mitochondrial proteins. *Plant Cell* 16: 241–256, 2004.
52. Heckler EJ, Rancy PC, Kodali VK, and Thorpe C. Generating disulfides with the Quiescin-sulfhydryl oxidases. *Biochim Biophys Acta* 1783: 567–577, 2008.
53. Heim R, Cubitt AB, and Tsien RY. Improved green fluorescence. *Nature* 373: 663–664, 1995.
54. Herald VL, Heazlewood JL, Day DA, and Millar AH. Proteomic identification of divalent metal cation binding proteins in plant mitochondria. *FEBS Lett* 537: 96–100, 2003.
55. Hogg PJ. Disulfide bonds as switches for protein function. *Trends Biochem Sci* 28: 210–214, 2003.
56. Hu J, Dong L, and Outten CE. The redox environment in the mitochondrial intermembrane space is maintained separately from the cytosol and matrix. *J Biol Chem* 283: 29126–29134, 2008.
57. Jiang K, Schwarzer C, Lally E, Zhang S, Ruzin S, Machen T, Remington SJ, and Feldman L. Expression and characterization of a redox-sensing green fluorescent protein (reduction-oxidation-sensitive green fluorescent protein) in *Arabidopsis*. *Plant Physiol* 141: 397–403, 2006.
58. Kim H, Melen K, Osterberg M, and von Heijne G. A global topology map of the *Saccharomyces cerevisiae* membrane proteome. *Proc Natl Acad Sci USA* 103: 11142–11147, 2006.
59. Klimova TA, Bell EL, Shroff EH, Weinberg FD, Snyder CM, Dimri GP, Schumacker PT, Budinger GRS, and Chandel NS. Hyperoxia-induced premature senescence requires p53

and pRb, but not mitochondrial matrix ROS. *FASEB J.* 23: 783–794, 2009.
60. Koch OR, Fusco S, Ranieri SC, Maulucci G, Palozza P, Larocca LM, Cravero AA, Farre' SM, De Spirito M, Galeotti T, and Pani G. Role of the life span determinant P66(shcA) in ethanol-induced liver damage. *Lab Invest* 88: 750–760, 2008.
61. Kolossov VL, Spring BQ, Sokolowski A, Conour JE, Clegg RM, Kenis PJ, and Gaskins HR. Engineering redox-sensitive linkers for genetically encoded FRET-based biosensors. *Exp Biol Med (Maywood)* 233: 238–248, 2008.
62. Kuner T and Augustine GJ. A genetically encoded ratiometric indicator for chloride: capturing chloride transients in cultured hippocampal neurons. *Neuron* 27: 447–459, 2000.
63. Lambeth JD. NOX enzymes and the biology of reactive oxygen. *Nat Rev Immunol* 4: 181–189, 2004.
64. Le Gall S, Neuhof A, and Rapoport T. The endoplasmic reticulum membrane is permeable to small molecules. *Mol Biol Cell* 15: 447–455, 2004.
65. Leshem Y, Melamed–Book N, Cagnac O, Ronen G, Nishri Y, Solomon M, Cohen G, and Levine A. Suppression of *Arabidopsis* vesicle-SNARE expression inhibited fusion of H_2O_2-containing vesicles with tonoplast and increased salt tolerance. *Proc Natl Acad Sci USA* 103: 18008–18013, 2006.
66. Llopis J, McCaffery JM, Miyawaki A, Farquhar MG, and Tsien RY. Measurement of cytosolic, mitochondrial, and Golgi pH in single living cells with green fluorescent proteins. *Proc Natl Acad Sci USA* 95: 6803–6808, 1998.
67. Lohman JR and Remington SJ. Development of a family of redox-sensitive green fluorescent protein indicators for use in relatively oxidizing subcellular environments. *Biochemistry* 47: 8678–8688, 2008.
68. Ma T, Vetrivel L, Yang H, Pedemonte N, Zegarra–Moran O, Galietta LJV, and Verkman AS. High-affinity activators of cystic fibrosis transmembrane conductance regulator (CFTR) chloride conductance identified by high-throughput screening. *J. Biol. Chem.* 277: 37235–37241, 2002.
69. Maeda K, Hagglund P, Finnie C, Svensson B, and Henriksen A. Structural basis for target protein recognition by the protein disulfide reductase thioredoxin. *Structure* 14: 1701–1710, 2006.
70. Markvicheva KN, Bogdanova EA, Staroverov DB, Lukyanov S, and Belousov VV. Imaging of intracellular hydrogen peroxide production with HyPer upon stimulation of HeLa cells with epidermal growth factor. *Methods Mol Biol* 476: 79–86, 2008.
71. Marty L, Siala W, Schwarzländer M, Fricker MD, Wirtz M, Sweetlove LJ, Meyer Y, Meyer AJ, Reichheld J–P, and Hell R. The NADPH-dependent thioredoxin system constitutes a functional backup for cytosolic glutathione reductase in *Arabidopsis*. *Proc Natl Acad Sci USA* 106: 9109–9114, 2009.
72. Mason JT, Kim SK, Knaff DB, and Wood MJ. Thermodynamic basis for redox regulation of the Yap1 signal transduction pathway. *Biochemistry* 45: 13409–13417, 2006.
73. Matthias LJ, Yam PT, Jiang XM, Vandegraaff N, Li P, Poumbourios P, Donoghue N, and Hogg PJ. Disulfide exchange in domain 2 of CD4 is required for entry of HIV-1. *Nat Immunol* 3: 727–732, 2002.
74. Matz MV, Fradkov AF, Labas YA, Savitsky AP, Zaraisky AG, Markelov ML, and Lukyanov SA. Fluorescent proteins from nonbioluminescent Anthozoa species. *Nat Biotechnol* 17: 969–973, 1999.
75. Maughan SC, Pasternak M, Cairns NG, Kiddle G, Brach T, Jarvis R, Haas F, Nieuwland J, Lim B, Müller C, Salcedo–Sora E, Kruse C, Orsel M, Hell R, Miller AJ, Bray P, Foyer CH, Murray JAH, Meyer AJ, and Cobbett CS. Plant homologs of the *Plasmodium falciparum* chloroquine-resistance transporter, *Pf*CRT, are required for glutathione homeostasis and stress responses. *Proc Natl Acad Sci USA* 107: 2331-2336, 2010.
76. Maulucci G, Labate V, Mele M, Panieri E, Arcovito G, Galeotti T, Ostergaard H, Winther JR, De Spirito M, and Pani G. High-resolution imaging of redox signaling in live cells through an oxidation-sensitive yellow fluorescent protein. *Sci Signal* 1: pl3, 2008.
77. Maulucci G, Pani G, Labate V, Mele M, Panieri E, Papi M, Arcovito G, Galeotti T, and De Spirito M. Investigation of the spatial distribution of glutathione redox-balance in live cells by using fluorescence ratio imaging microscopy. *Biosens Bioelectron* 25: 682–687, 2009.
78. Meech SR. Excited state reactions in fluorescent proteins. *Chem Soc Rev* 38: 2922–2934, 2009.
79. Merksamer PI, Trusina A, and Papa FR. Real-time redox measurements during endoplasmic reticulum stress reveal interlinked protein folding functions. *Cell* 135: 933–947, 2008.
80. Meyer AJ. The integration of glutathione homeostasis and redox signaling. *J Plant Physiol* 165: 1390–1403, 2008.
81. Meyer AJ, Brach T, Marty L, Kreye S, Rouhier N, Jacquot JP, and Hell R. Redox-sensitive GFP in *Arabidopsis thaliana* is a quantitative biosensor for the redox potential of the cellular glutathione redox buffer. *Plant J* 52: 973–986, 2007.
82. Mieyal JJ, Gallogly MM, Qanungo S, Sabens EA, and Shelton MD. Molecular mechanisms and clinical implications of reversible protein S-glutathionylation. *Antioxid Redox Signal* 10: 1941–1988, 2008.
83. Miller EW, Albers AE, Pralle A, Isacoff EY, and Chang CJ. Boronate-based fluorescent probes for imaging cellular hydrogen peroxide. *J Am Chem Soc* 127: 16652–16659, 2005.
84. Miller EW, Bian SX, and Chang CJ. A fluorescent sensor for imaging reversible redox cycles in living cells. *J Am Chem Soc* 129: 3458–3459, 2007.
85. Miller EW and Chang CJ. Fluorescent probes for nitric oxide and hydrogen peroxide in cell signaling. *Curr Opin Chem Biol* 11: 620–625, 2007.
86. Miller EW, Tulyanthan O, Isacoff EY, and Chang CJ. Molecular imaging of hydrogen peroxide produced for cell signaling. *Nat Chem Biol* 3: 263–267, 2007.
87. Morgan MJ, Lehmann M, Schwarzländer M, Baxter CJ, Sienkiewicz–Porzucek A, Williams TCR, Schauer N, Fernie AR, Fricker MD, Ratcliffe RG, Sweetlove LJ, and Finkemeier I. Decrease in manganese superoxide dismutase leads to reduced root growth and affects tricarboxylic acid cycle flux and mitochondrial redox homeostasis. *Plant Physiol* 147: 101–114, 2008.
88. Mravec J, Skupa P, Bailly A, Hoyerova K, Krecek P, Bielach A, Petrasek J, Zhang J, Gaykova V, Stierhof Y-D, Dobrev PI, Schwarzerova K, Rolcik J, Seifertova D, Luschnig C, Benkova E, Zazimalova E, Geisler M, and Friml J. Subcellular homeostasis of phytohormone auxin is mediated by the ER-localized PIN5 transporter. *Nature* 459: 1136–1140, 2009.
89. Nagai T, Sawano A, Park ES, and Miyawaki A. Circularly permuted green fluorescent proteins engineered to sense Ca^{2+}. *Proc Natl Acad Sci USA* 98: 3197–3202, 2001.
90. Niethammer P, Grabher C, Look AT, and Mitchison TJ. A tissue-scale gradient of hydrogen peroxide mediates rapid wound detection in zebrafish. *Nature* 459: 996–999, 2009.
91. Ormö M, Cubitt AB, Kallio K, Gross LA, Tsien RY, and Remington SJ. Crystal structure of the *Aequorea victoria* green fluorescent protein. *Science* 273: 1392–1395, 1996.

92. Ostergaard H, Henriksen A, Hansen FG, and Winther JR. Shedding light on disulfide bond formation: Engineering a redox switch in green fluorescent protein. *EMBO J* 20: 5853–5862, 2001.
93. Ostergaard H, Tachibana C, and Winther JR. Monitoring disulfide bond formation in the eukaryotic cytosol. *J Cell Biol* 166: 337–345, 2004.
94. Owusu-Ansah E and Banerjee U. Reactive oxygen species prime *Drosophila* haematopoietic progenitors for differentiation. *Nature* 461: 537–541, 2009.
95. Paige JS, Xu G, Stancevic B, and Jaffrey SR. Nitrosothiol reactivity profiling identifies S-nitrosylated proteins with unexpected stability. *Chem Biol* 15: 1307–1316, 2008.
96. Pan S and Berk BC. Glutathiolation regulates tumor necrosis factor-alpha-induced caspase-3 cleavage and apoptosis: Key role for glutaredoxin in the death pathway. *Circ Res* 100: 213–219, 2007.
97. Pasternak M, Lim B, Wirtz M, Hell R, Cobbett CS, and Meyer AJ. Restricting glutathione biosynthesis to the cytosol is sufficient for normal plant development. *Plant J* 53: 999–1012, 2008.
98. Peltoniemi MJ, Karala AR, Jurvansuu JK, Kinnula VL, and Ruddock LW. Insights into deglutathionylation reactions: Different intermediates in the glutaredoxin and protein disulphide isomerase catalysed reactions are defined by the gamma-linkage present in glutathione. *J Biol Chem* 281: 33107–33114, 2006.
99. Ristow M, Zarse K, Oberbach A, Kloting N, Birringer M, Kiehntopf M, Stumvoll M, Kahn CR, and Bluher M. Antioxidants prevent health-promoting effects of physical exercise in humans. *Proc Natl Acad Sci USA* 106: 8665–8670, 2009.
100. Robin E, Guzy RD, Loor G, Iwase H, Waypa GB, Marks JD, Hoek TL, and Schumacker PT. Oxidant stress during simulated ischemia primes cardiomyocytes for cell death during reperfusion. *J Biol Chem* 282: 19133–19143, 2007.
101. Romero–Puertas MC, Corpas FJ, Sandalio LM, Leterrier M, Rodriguez–Serrano M, del Rio LA, and Palma JM. Glutathione reductase from pea leaves: Response to abiotic stress and characterization of the peroxisomal isozyme. *New Phytologist* 170: 43–52, 2006.
102. Rota C, Chignell CF, and Mason RP. Evidence for free radical formation during the oxidation of 2′-7′-dichlorofluorescin to the fluorescent dye 2′-7′-dichlorofluorescein by horseradish peroxidase: possible implications for oxidative stress measurements. *Free Radic Biol Med* 27: 873–881, 1999.
103. Schafer FQ and Buettner GR. Redox environment of the cell as viewed through the redox state of the glutathione disulfide/glutathione couple. *Free Radic Biol Med* 30: 1191–1212, 2001.
104. Schafer ZT, Grassian AR, Song L, Jiang Z, Gerhart–Hines Z, Irie HY, Gao S, Puigserver P, and Brugge JS. Antioxidant and oncogene rescue of metabolic defects caused by loss of matrix attachment. *Nature* 461: 109–113, 2009.
105. Schmidt B, Ho L, and Hogg PJ. Allosteric disulfide bonds. *Biochemistry* 45: 7429–7433, 2006.
106. Schwarzer C, Illek B, Suh JH, Remington SJ, Fischer H, and Machen TE. Organelle redox of CF and CFTR-corrected airway epithelia. *Free Radic Biol Med* 43: 300–316, 2007.
107. Schwarzländer M, Fricker MD, Müller C, Marty L, Brach T, Novak J, Sweetlove LJ, Hell R, and Meyer AJ. Confocal imaging of glutathione redox potential in living plant cells. *J Microsc* 231: 299–316, 2008.
108. Schwarzländer M, Fricker MD, and Sweetlove LJ. Monitoring the *in vivo* redox state of plant mitochondria: Effect of respiratory inhibitors, abiotic stress and assessment of recovery from oxidative challenge. *Biochim Biophys Acta* 1787: 468–475, 2009.
109. Sevier CS and Kaiser CA. Ero1 and redox homeostasis in the endoplasmic reticulum. *Biochim Biophys Acta* 1783: 549-556, 2008.
110. Shimaoka T, Miyake C, and Yokota A. Mechanism of the reaction catalyzed by dehydroascorbate reductase from spinach chloroplasts. *Eur J Biochem* 270: 921–928, 2003.
111. Shimomura O, Johnson FH, and Saiga Y. Extraction, purification and properties of aequorin, a bioluminescent protein from the luminous hydromedusan, *Aequorea*. *J Cell Comp Physiol* 59: 223–239, 1962.
112. Song JJ, Rhee JG, Suntharalingam M, Walsh SA, Spitz DR, and Lee YJ. Role of glutaredoxin in metabolic oxidative stress. Glutaredoxin as a sensor of oxidative stress mediated by H2O2. *J Biol Chem* 277: 46566–46575, 2002.
113. Stewart EJ, Aslund F, and Beckwith J. Disulfide bond formation in the *Escherichia coli* cytoplasm: An *in vivo* role reversal for the thioredoxins. *EMBO J* 17: 5543–5550, 1998.
114. Sun X, Shih AY, Johannssen HC, Erb H, Li P, and Murphy TH. Two-photon imaging of glutathione levels in intact brain indicates enhanced redox buffering in developing neurons and cells at the cerebrospinal fluid and blood-brain interface. *J Biol Chem* 281: 17420–17431, 2006.
115. Tarpey MM, Wink DA, and Grisham MB. Methods for detection of reactive metabolites of oxygen and nitrogen: *In vitro* and *in vivo* considerations. *Am J Physiol Regul Integr Comp Physiol* 286: R431–444, 2004.
116. Trzcinska–Daneluti AM, Ly D, Huynh L, Jiang C, Fladd C, and Rotin D. High-content functional screen to identify proteins that correct F508del-CFTR function. *Mol Cell Proteomics* 8: 780–790, 2009.
117. Tsien RY. The green fluorescent protein. *Annu Rev Biochem* 67: 509–544, 1998.
118. Tu BP, Ho–Schleyer SC, Travers KJ, and Weissman JS. Biochemical basis of oxidative protein folding in the endoplasmic reticulum. *Science* 290: 1571–1574, 2000.
119. Veal EA, Day AM, and Morgan BA. Hydrogen peroxide sensing and signaling. *Mol Cell* 26: 1–14, 2007.
120. Vernoux T, Wilson RC, Seeley KA, Reichheld JP, Muroy S, Brown S, Maughan SC, Cobbett CS, Van Montagu M, Inze D, May MJ, and Sung ZR. The ROOT MERISTEMLESS1/CADMIUM SENSITIVE2 gene defines a glutathione-dependent pathway involved in initiation and maintenance of cell division during postembryonic root development. *Plant Cell* 12: 97–110, 2000.
121. Vesce S, Jekabsons MB, Johnson–Cadwell LI, and Nicholls DG. Acute glutathione depletion restricts mitochondrial ATP export in cerebellar granule neurons. *J Biol Chem* 280: 38720–38728, 2005.
122. von Heijne G. Membrane-protein topology. *Nat Rev Mol Cell Biol* 7: 909–918, 2006.
123. Wachter A, Wolf S, Steininger H, Bogs J, and Rausch T. Differential targeting of GSH1 and GSH2 is achieved by multiple transcription initiation: Implications for the compartmentation of glutathione biosynthesis in the *Brassicaceae*. *Plant J* 41: 15–30, 2005.
124. Wachter RM, Elsliger MA, Kallio K, Hanson GT, and Remington SJ. Structural basis of spectral shifts in the yellow-emission variants of green fluorescent protein. *Structure* 6: 1267–1277, 1998.
125. Wachter RM, Yarbrough D, Kallio K, and Remington SJ. Crystallographic and energetic analysis of binding of se-

lected anions to the yellow variants of green fluorescent protein. *J Mol Biol* 301: 157–171, 2000.
126. Wang W, Fang H, Groom L, Cheng A, Zhang W, Liu J, Wang X, Li K, Han P, Zheng M, Yin J, Mattson MP, Kao JP, Lakatta EG, Sheu SS, Ouyang K, Chen J, Dirksen RT, and Cheng H. Superoxide flashes in single mitochondria. *Cell* 134: 279–290, 2008.
127. Wardman P. Reduction potentials of one-electron couples involving free radicals in aqueous solution. *J Phys Chem Ref Data* 18: 1637–1755, 1989.
128. Watson WH, Pohl J, Montfort WR, Stuchlik O, Reed MS, Powis G, and Jones DP. Redox potential of human Thioredoxin 1 and identification of a second dithiol/disulfide motif. *J Biol Chem* 278: 33408–33415, 2003.
129. Wiita AP, Perez–Jimenez R, Walther KA, Grater F, Berne BJ, Holmgren A, Sanchez–Ruiz JM, and Fernandez JM. Probing the chemistry of thioredoxin catalysis with force. *Nature* 450: 124–127, 2007.
130. Winterbourn CC. Reconciling the chemistry and biology of reactive oxygen species. *Nat Chem Biol* 4: 278–286, 2008.
131. Winterbourn CC and Metodiewa D. Reactivity of biologically important thiol compounds with superoxide and hydrogen peroxide. *Free Radic Biol Med* 27: 322–328, 1999.
132. Wouters MA, Lau KK, and Hogg PJ. Cross-strand disulphides in cell entry proteins: poised to act. *Bioessays* 26: 73–79, 2004.
133. Yang F, Moss LG, and Phillips GN. The molecular structure of green fluorescent protein. *Nat Biotechnol* 14: 1246–1251, 1996.
134. Young PR, Connors White AL, and Dzido GA. Kinetic analysis of the intracellular conjugation of monochlorobimane by IC-21 murine macrophage glutathione-S-transferase. *Biochim Biophys Acta* 1201: 461–465, 1994.
135. Zacharias DA and Tsien RY. Molecular biology and mutation of green fluorescent protein. *Methods Biochem Anal* 47: 83–120, 2006.
136. Zheng M, Aslund F, and Storz G. Activation of the OxyR transcription factor by reversible disulfide bond formation. *Science* 279: 1718–1721, 1998.
137. Zheng X, Yang Z, Yue Z, Alvarez JD, and Sehgal A. FOXO and insulin signaling regulate sensitivity of the circadian clock to oxidative stress. *Proc Natl Acad Sci USA* 104: 15899–15904, 2007.

Address correspondence to:
Tobias P. Dick
German Cancer Research Center
DKFZ-ZMBH Alliance
Im Neuenheimer Feld 280
D-69120 Heidelberg
Germany

E-mail: t.dick@dkfz.de

Date of first submission to ARS Central, October 12, 2009; date of final revised submission, January 18, 2010; date of acceptance, January 20, 2010.

Abbreviations Used

AA = ascorbic acid
BASI = barley α-amylase/subtilisin inhibitor
BMES = bis(2-mercaptoethyl)sulfone
BSO = L-buthionine (*S,R*)-sulfoximine
CFP = cyan fluorescent protein
cpYFP = circularly-permuted YFP
DCF = 2′,7′-dichlorofluorescein
DHA = dehydroascorbate
DHAR = dehydroascorbate reductase
DIC = dicarboxylate carrier
DTNB = 5,5′-dithiobis(2-nitrobenzoic acid)
DTT = dithiothreitol
$E^{\circ\prime}$ = midpoint redox potential under standard conditions
ECFP = enhanced CFP
EGFP = enhanced GFP
E_{GSH} = glutathione redox potential
ER = endoplasmic reticulum
ESPT = excited state proton transfer
FACS = fluorescence-activated cell sorting
FP = fluorescent protein
FRET = fluorescence resonance energy transfer
γ-EC = γ-glutamylcysteine
GFP = green fluorescent protein
GR = glutathione reductase
Grx = glutaredoxin
GSH = reduced glutathione
GSN = *S*-nitrosoglutathione
GSSG = glutathione disulfide
GST = glutathione S-transferase
H_2DCF = 2′,7′-dihydrodichlorofluorescein
H_2O_2 = hydrogen peroxide
HPLC = high pressure liquid chromatography
HTS = high throughput screening
IMS = intermembrane space
MCB = monochlorobimane
MDHA = monodehydroascorbate
$NADP^+$ = nicotinamide adenine dinucleotide phosphate (oxidized)
NADPH = nicotinamide adenine dinucleotide phosphate (reduced)
$NO^\bullet$ = nitric oxide
$O_2^{\bullet-}$ = superoxide
OCG = 2-oxoglutarate carrier
$ONOO^-$ = peroxynitrite
OxD = degree of oxidation
PDB = protein data bank
PDI = protein disulfide isomerase
PET = photosynthetic electron transport
PF1 = peroxyfluor-1
PR1 = peroxyresorufin-1
PX1 = peroxyxanthone-1
RD = regulatory domain
ReTA = redox-based topology analysis
RF1 = redoxfluor-1
RFP = red fluorescent protein
roGFP = redox-sensitive GFP
ROS = reactive oxygen species
rxYFP = redox-sensitive YFP
SOD = superoxide dismutase
TM = transmembrane
TMD = transmembrane domain
TRAIL = TNF-related apoptosis inducing ligand
Trx = thioredoxin
wtGFP = wild-type GFP
YFP = yellow fluorescent protein